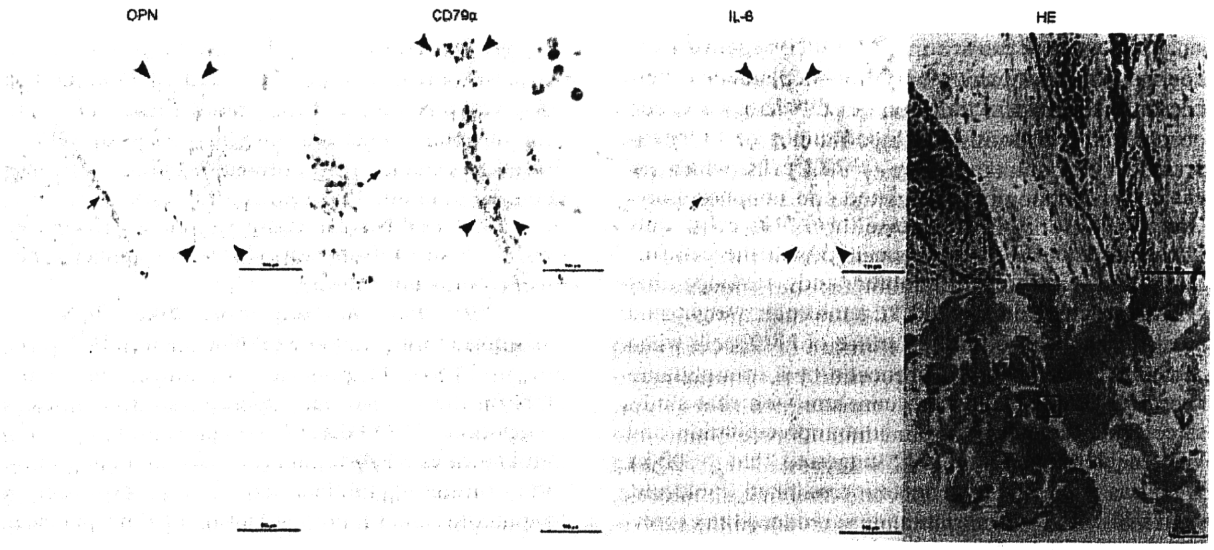

Figure 5. Immunohistochemical analysis of rheumatoid arthritis (RA) synovium. One of the synovial villi in the inflamed joint of a patient with RA was evaluated by hematoxylin and eosin (H&E) staining. The H&E-stained image in the upper right panel is a higher-magnification view of the boxed area in the lower right panel. The RA synovium samples in the other 3 upper panels were stained with the antibody against osteopontin (anti-OPN) (O-17), anti–pan B cell antigen CD79α, and anti–interleukin-6 (anti–IL-6) antibodies. The corresponding panels below were stained with class-matched normal IgG as a negative control. The appearance of IL-6–positive cells coincided with the site at which OPN and B lymphocytes colocalized (**arrowheads**), whereas IL-6 was not detected in areas where only OPN-positive cells were distributed or at sites far from clusters of B lymphocytes (**arrows**).

sublining region, and some of these B lymphocyte clusters were surrounded by OPN-positive cells. IL-6–positive cells were scattered in the sublining region, as has been reported previously (44).

Of note, some of the areas of distribution of IL-6–positive cells coincided with sites at which OPN and B lymphocytes colocalized (indicated by arrowheads in Figure 5). However, IL-6 was not detected in areas where only OPN-positive cells were distributed or at sites far from clusters of B lymphocytes (indicated by arrows in Figure 5).

DISCUSSION

The present study revealed a new role of OPN in the RA synovium, using primary cultured FLS derived from RA patients to analyze the function of FLS-expressed native OPN. A specifically modified 75-kd OPN was predominantly expressed by RA FLS and was associated with significantly elevated IL-6 production in FLS–B lymphocyte cocultures. The 75-kd OPN formed a >200-kd OPN/fibronectin–crosslinked molecule via transglutamination, which was detected on the synovial cell surface, resulting in exposure of its thrombin-cleaved neoepitope. This >200-kd cell surface OPN affected the interactions between FLS and B lymphocytes by supporting adhesion of B lymphocytes to FLS in FLS–B lymphocyte cocultures, and consequently IL-6 production was enhanced. This FLS–B lymphocyte interaction also appeared to occur in vivo.

OPN by itself weighs 37 kd, as determined previously using mass spectrometry (25), but due to its various posttranslational modifications, the migration of full-length OPN, detected on SDS-PAGE, differs among cell types within ~45–80 kd (42). Accordingly, our results from Western blotting of OPN showed multiple bands with different molecular weights. In particular, a single band at 75 kd that was detected predominantly in RA FLS suggested that this specifically modified 75-kd OPN was worth investigating to determine the function of OPN in RA.

In fact, the localization of OPN was different between 75-kd OPN–negative and 75-kd OPN–positive FLS. The existence of >200-kd OPN in the cell surface fraction of 75-kd OPN–positive FLS on Western blotting, and the staining pattern of OPN on immunofluorescence assay of these FLS, showing the cell outline distribution, suggested that OPN was associated with the cell surface side of the plasma membrane. These distinct

findings were considered attributable to 75-kd OPN, since they were negative in 75-kd OPN–negative FLS. Such posttranslational modification–dependent differences in subcellular localization of OPN have also been observed in previously published studies of OPN expressed by normal rat kidney (NRK) cells, which revealed that among phosphorylated and nonphosphorylated forms of OPN expressed by NRK cells, only phosphorylated OPN was associated with the cell surface (19,23). Moreover, another study revealed that OPN was detected at >200 kd molecular weight and found to be localized on the surface of NRK cells when covalently crosslinked to fibronectin by a transglutaminase (26). Our results were consistent with that study, since the observations from immunoprecipitation and Western blotting of the FLS suggested that >200-kd OPN was an OPN/fibronectin-crosslinked molecule, and inhibition of a transglutaminase reduced the expression of >200-kd OPN. Considering these facts together, >200-kd OPN could be considered an OPN/fibronectin–covalently crosslinked molecule synthesized by a transglutaminase from 75-kd OPN.

In contrast, >200-kd cell surface OPN was poorly detected in 75-kd OPN–negative FLS. Moreover, overexpression of OPN by 75-kd OPN–negative FLS only increased the expression of 54-kd OPN, and did not induce expression of 75-kd OPN nor did it alter the expression of >200-kd OPN, suggesting that there might be an unknown enzyme in 75-kd OPN–positive FLS that performs the specific modifications of 75-kd OPN necessary for it to associate with the cell surface and to form the >200-kd OPN/fibronectin–crosslinked molecule.

To assess the relevance of 75-kd OPN in RA, we performed cocultures of FLS and B lymphocytes. Previous studies have revealed that FLS–B lymphocyte coculture allows the adhesion of B lymphocytes to FLS, which induces cell–cell interactions between FLS and B lymphocytes and, consequently, increases the production of several cytokines, including IL-6 (9,12), but the mechanism has not been elucidated. We focused on IL-6 production in FLS–B lymphocyte cocultures and found that increased IL-6 production was associated with the existence of 75-kd OPN, which suggested that 75-kd OPN together with cell–cell interactions between FLS and B lymphocytes can enhance IL-6 production. We also revealed that among FLS and B lymphocytes, FLS were the dominant cell type for IL-6 production in coculture, as was shown in experiments involving knockdown of IL-6 in FLS.

To examine whether 75-kd OPN could enhance IL-6 production, we performed overexpression and knockdown of OPN in FLS, which demonstrated that IL-6 production was increased and decreased in accordance with the increase and decrease of 75-kd OPN and >200-kd OPN, respectively. Among these 2 OPN forms with different molecular weights, >200-kd OPN appeared to enhance IL-6 production, since the transglutaminase inhibitor that reduced the expression of only the >200-kd OPN significantly suppressed IL-6 production in 75-kd OPN–positive FLS–B lymphocyte cocultures (results not shown).

We then analyzed how 75-kd OPN or its crosslinked form, >200-kd OPN, enhanced IL-6 production in FLS–B lymphocyte cocultures. The >200-kd OPN on the cell surface exposed its thrombin-cleaved neoepitope, SVVYGLR (27), a ligand for integrin $\alpha 4\beta 1$, also known as VLA-4, integrin $\alpha 9\beta 1$, and integrin $\alpha 4\beta 7$ (30). Considering the fact that VLA-4 is expressed by B lymphocytes and supports adhesion of B lymphocytes to FLS in FLS–B lymphocyte coculture (12), >200-kd OPN was indicated as the ligand for VLA-4, which acts as an adhesion molecule. This idea was supported by the results from our B lymphocyte adhesion assay with a blocking antibody against OPN, and by the fact that the transglutaminase inhibitor also suppressed adhesion of B lymphocytes to FLS (results not shown). Meanwhile,

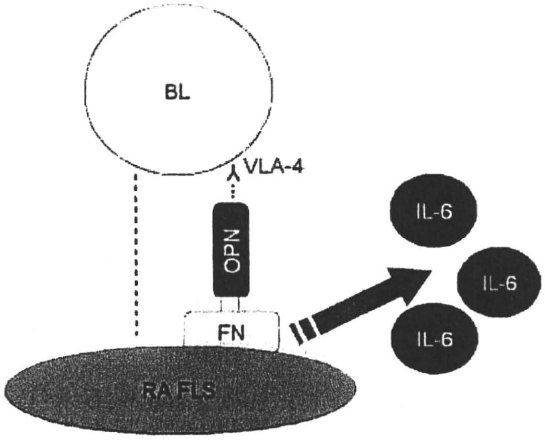

Figure 6. Diagram of the in vitro findings, showing cell–cell interactions between fibroblast-like synoviocytes (FLS) and B lymphocytes (BL). RA FLS were characterized by the expression of 75-kd OPN, from which a transglutaminase synthesized the >200-kd OPN/fibronectin (FN)–crosslinked molecule that was localized on the synovial cell surface in its thrombin-cleaved form. This cell surface OPN mediated cell–cell interactions between OPN and B lymphocytes by supporting adhesion of B lymphocytes to FLS through very late activation antigen 4 (VLA-4) and enhanced IL-6 production. An unknown link between FLS and B lymphocytes is also shown. See Figure 5 for other definitions.

integrin $\alpha4\beta7$, which was also expressed by B lymphocytes, did not mediate such adhesion (12).

VCAM-1, which was expressed by FLS and also supports B lymphocyte adhesion, possibly through VLA-4 (11), was detected in equal amounts among RA and non-RA FLS (results not shown). Therefore, we postulated that integrin $\alpha4\beta7$ and VCAM-1 were not involved in the adhesion of B lymphocytes to FLS or subsequent IL-6 production, and that such adhesion was mediated by >200-kd OPN and VLA-4, which would further initiate the cell–cell interaction between FLS and B lymphocytes, leading to IL-6 production.

Our findings suggested that, in response to these FLS–B lymphocyte interactions, FLS boosted their IL-6 production. Similar studies on cell–cell interactions between FLS and T lymphocytes have shown that lymphocyte function–associated antigen 1, intercellular adhesion molecule 2, and the ezrin/Akt pathway are involved in their interaction, which also enhances IL-6 production (2). Thus, this pathway may also be involved in FLS–B lymphocyte interactions, although further investigation is needed to fully elucidate the mechanism.

In summary, the findings from these in vitro experiments showed that RA FLS are characterized by the expression of 75-kd OPN. This was the substrate of a transglutaminase that formed the >200-kd OPN/fibronectin–crosslinked molecule, a molecule localized on the surface of FLS in its thrombin-cleaved form. This surface OPN mediated cell–cell interactions between FLS and B lymphocytes, and enhanced IL-6 production (Figure 6). Moreover, such FLS–B lymphocyte interactions, or interactions between FLS-expressing OPN and B lymphocytes stimulating IL-6 production, appeared to take place in vivo, as shown by immunohistochemistry. Taking into account the previously reported findings on the pathogenic significance of IL-6 (45), B lymphocytes (46,47), VLA-4 (48), and the thrombin-cleaved neoepitope of OPN (32,33) in RA, the present study revealed a novel role of OPN in RA.

Regarding the weaknesses of this study, we need to mention the discrepancy in the findings between RA FLS and 75-kd OPN–positive FLS. Since 75-kd OPN was detected in all 10 RA FLS, but also in 3 non-RA FLS, it was not specific to RA FLS. There is no doubt that 75-kd OPN enhanced IL-6 production in FLS–B lymphocyte cocultures and appeared to aggravate chronic inflammation in vivo. However, it should not be considered the cause of RA; rather, we could postulate that it is one of several molecules with induced expression in arthritis and is involved in the chronic progression of arthritis by stimulating IL-6 production. This is supported by the observation that, in the joint tissue of a non-RA donor, the FLS expressed amounts of 75-kd OPN comparable with those in RA FLS, and showed severe synovitis at the time of surgery.

We also have to note that the mechanism involved in the modification of 75-kd OPN has not been defined, and the responsible transglutaminase has not been identified. Further investigations in this area would be required for better understanding of the pathology of RA. Nevertheless, our results show that a specifically modified 75-kd form of OPN was expressed by RA FLS. This form of OPN affected cell–cell interactions between FLS and B lymphocytes by supporting the adhesion of B lymphocytes to FLS. As a result, IL-6 production was enhanced in FLS–B lymphocyte cocultures.

AUTHOR CONTRIBUTIONS

All authors were involved in drafting the article or revising it critically for important intellectual content, and all authors approved the final version to be published. Dr. Nakata had full access to all of the data in the study and takes responsibility for the integrity of the data and the accuracy of the data analysis.

Study conception and design. Nakata, Ochi, Yoshikawa.

Acquisition of data. Take, Nakata, Nishimoto.

Analysis and interpretation of data. Take, Nakata, Hashimoto, Tsuboi, Nishimoto.

REFERENCES

1. Huber LC, Distler O, Tarner I, Gay RE, Gay S, Pap T. Synovial fibroblasts: key players in rheumatoid arthritis. Rheumatology (Oxford) 2006;45:669–75.
2. Singh K, Colmegna I, He X, Weyand CM, Goronzy JJ. Synoviocyte stimulation by the LFA-1-intercellular adhesion molecule-2-ezrin-Akt pathway in rheumatoid arthritis. J Immunol 2008;180:1971–8.
3. Tran CN, Lundy SK, White PT, Endres JL, Motyl CD, Gupta R, et al. Molecular interactions between T cells and fibroblast-like synoviocytes: role of membrane tumor necrosis factor-α on cytokine-activated T cells. Am J Pathol 2007;171:1588–98.
4. Vallejo AN, Yang H, Klimiuk PA, Weyand CM, Goronzy JJ. Synoviocyte-mediated expansion of inflammatory T cells in rheumatoid synovitis is dependent on CD47-thrombospondin 1 interaction. J Immunol 2003;171:1732–40.
5. Chomarat P, Rissoan MC, Pin JJ, Banchereau J, Miossec P. Contribution of IL-1, CD14, and CD13 in the increased IL-6 production induced by in vitro monocyte-synoviocyte interactions. J Immunol 1995;155:3645–52.
6. Bombara MP, Webb DL, Conrad P, Marlor CW, Sarr T, Ranges GE, et al. Cell contact between T cells and synovial fibroblasts causes induction of adhesion molecules and cytokines. J Leukoc Biol 1993;54:399–406.
7. Blue ML, Conrad P, Webb DL, Sarr T, Macaro M. Interacting monocytes and synoviocytes induce adhesion molecules by a cytokine-regulated process. Lymphokine Cytokine Res 1993;12:213–8.
8. Shimaoka Y, Attrep JF, Hirano T, Ishihara K, Suzuki R, Toyosaki T, et al. Nurse-like cells from bone marrow and synovium of patients with rheumatoid arthritis promote survival and enhance function of human B cells. J Clin Invest 1998;102:606–18.

9. Takeuchi E, Tomita T, Toyosaki-Maeda T, Kaneko M, Takano H, Hashimoto H, et al. Establishment and characterization of nurse cell–like stromal cell lines from synovial tissues of patients with rheumatoid arthritis. Arthritis Rheum 1999;42:221–8.
10. Hayashida K, Shimaoka Y, Ochi T, Lipsky PE. Rheumatoid arthritis synovial stromal cells inhibit apoptosis and up-regulate Bcl-xL expression by B cells in a CD49/CD29-CD106-dependent mechanism. J Immunol 2000;164:1110–6.
11. Burger JA, Zvaifler NJ, Tsukada N, Firestein GS, Kipps TJ. Fibroblast-like synoviocytes support B-cell pseudoemperipolesis via a stromal cell-derived factor-1- and CD106 (VCAM-1)-dependent mechanism. J Clin Invest 2001;107:305–15.
12. Takeuchi E, Tanaka T, Umemoto E, Tomita T, Shi K, Takahi K, et al. VLA-4-dependent and -independent pathways in cell contact-induced proinflammatory cytokine production by synovial nurse-like cells from rheumatoid arthritis patients. Arthritis Res 2002;4:R10–7.
13. Tani-Ishii N, Tsunoda A, Umemoto T. Osteopontin antisense deoxyoligonucleotides inhibit bone resorption by mouse osteoclasts in vitro. J Periodontal Res 1997;32:480–6.
14. Dodds RA, Connor JR, James IE, Rykaczewski EL, Appelbaum E, Dul E, et al. Human osteoclasts, not osteoblasts, deposit osteopontin onto resorption surfaces: an in vitro and ex vivo study of remodeling bone. J Bone Miner Res 1995;10:1666–80.
15. Horton MA, Nesbit MA, Helfrich MH. Interaction of osteopontin with osteoclast integrins. Ann N Y Acad Sci 1995;760:190–200.
16. Lampe MA, Patarca R, Iregui MV, Cantor H. Polyclonal B cell activation by the Eta-1 cytokine and the development of systemic autoimmune disease. J Immunol 1991;147:2902–6.
17. Patarca R, Freeman GJ, Singh RP, Wei FY, Durfee T, Blattner F, et al. Structural and functional studies of the early T lymphocyte activation 1 (Eta-1) gene: definition of a novel T cell-dependent response associated with genetic resistance to bacterial infection. J Exp Med 1989;170:145–61.
18. Patarca R, Wei FY, Singh P, Morasso MI, Cantor H. Dysregulated expression of the T cell cytokine Eta-1 in CD4-8- lymphocytes during the development of murine autoimmune disease. J Exp Med 1990;172:1177–83.
19. Nemir M, DeVouge MW, Mukherjee BB. Normal rat kidney cells secrete both phosphorylated and nonphosphorylated forms of osteopontin showing different physiological properties. J Biol Chem 1989;264:18202–8.
20. Weber GF, Zawaideh S, Hikita S, Kumar VA, Cantor H, Ashkar S. Phosphorylation-dependent interaction of osteopontin with its receptors regulates macrophage migration and activation. J Leukoc Biol 2002;72:752–61.
21. Shanmugam V, Chackalaparampil I, Kundu GC, Mukherjee AB, Mukherjee BB. Altered sialylation of osteopontin prevents its receptor-mediated binding on the surface of oncogenically transformed tsB77 cells. Biochemistry 1997;36:5729–38.
22. Christensen B, Kazanecki CC, Petersen TE, Rittling SR, Denhardt DT, Sorensen ES. Cell type-specific post-translational modifications of mouse osteopontin are associated with different adhesive properties. J Biol Chem 2007;282:19463–72.
23. Singh K, DeVouge MW, Mukherjee BB. Physiological properties and differential glycosylation of phosphorylated and nonphosphorylated forms of osteopontin secreted by normal rat kidney cells. J Biol Chem 1990;265:18696–701.
24. He B, Mirza M, Weber GF. An osteopontin splice variant induces anchorage independence in human breast cancer cells. Oncogene 2006;25:2192–202.
25. Keykhosravani M, Doherty-Kirby A, Zhang C, Brewer D, Goldberg HA, Hunter GK, et al. Comprehensive identification of post-translational modifications of rat bone osteopontin by mass spectrometry. Biochemistry 2005;44:6990–7003.
26. Beninati S, Senger DR, Cordella-Miele E, Mukherjee AB, Chackalaparampil I, Shanmugam V, et al. Osteopontin: its transglutaminase-catalyzed posttranslational modifications and cross-linking to fibronectin. J Biochem 1994;115:675–82.
27. Senger DR, Perruzzi CA, Papadopoulos-Sergiou A, Van de Water L. Adhesive properties of osteopontin: regulation by a naturally occurring thrombin-cleavage in close proximity to the GRGDS cell-binding domain. Mol Biol Cell 1994;5:565–74.
28. Agnihotri R, Crawford HC, Haro H, Matrisian LM, Havrda MC, Liaw L. Osteopontin, a novel substrate for matrix metalloproteinase-3 (stromelysin-1) and matrix metalloproteinase-7 (matrilysin). J Biol Chem 2001;276:28261–7.
29. Yumoto K, Ishijima M, Rittling SR, Tsuji K, Tsuchiya Y, Kon S, et al. Osteopontin deficiency protects joints against destruction in anti-type II collagen antibody-induced arthritis in mice. Proc Natl Acad Sci U S A 2002;99:4556–61.
30. Bayless KJ, Meininger GA, Scholtz JM, Davis GE. Osteopontin is a ligand for the $\alpha 4\beta 1$ integrin. J Cell Sci 1998;111:1165–74.
31. Yokosaki Y, Matsuura N, Sasaki T, Murakami I, Schneider H, Higashiyama S, et al. The integrin $\alpha(9)\beta(1)$ binds to a novel recognition sequence (SVVYGLR) in the thrombin-cleaved amino-terminal fragment of osteopontin. J Biol Chem 1999;274:36328–34.
32. Yamamoto N, Sakai F, Kon S, Morimoto J, Kimura C, Yamazaki H, et al. Essential role of the cryptic epitope SLAYGLR within osteopontin in a murine model of rheumatoid arthritis. J Clin Invest 2003;112:181–8.
33. Yamamoto N, Nakashima T, Torikai M, Naruse T, Morimoto J, Kon S, et al. Successful treatment of collagen-induced arthritis in non-human primates by chimeric anti-osteopontin antibody. Int Immunopharmacol 2007;7:1460–70.
34. Petrow PK, Hummel KM, Schedel J, Franz JK, Klein CL, Muller-Ladner U, et al. Expression of osteopontin messenger RNA and protein in rheumatoid arthritis: effects of osteopontin on the release of collagenase 1 from articular chondrocytes and synovial fibroblasts. Arthritis Rheum 2000;43:1597–605.
35. Ohshima S, Yamaguchi N, Nishioka K, Mima T, Ishii T, Umeshita-Sasai M, et al. Enhanced local production of osteopontin in rheumatoid joints. J Rheumatol 2002;29:2061–7.
36. Hasegawa M, Nakoshi Y, Iino T, Sudo A, Segawa T, Maeda M, et al. Thrombin-cleaved osteopontin in synovial fluid of subjects with rheumatoid arthritis. J Rheumatol 2009;36:240–5.
37. Xu G, Nie H, Li N, Zheng W, Zhang D, Feng G, et al. Role of osteopontin in amplification and perpetuation of rheumatoid synovitis. J Clin Invest 2005;115:1060–7.
38. Arnett FC, Edworthy SM, Bloch DA, McShane DJ, Fries JF, Cooper NS, et al. The American Rheumatism Association 1987 revised criteria for the classification of rheumatoid arthritis. Arthritis Rheum 1988;31:315–24.
39. Wiznerowicz M, Trono D. Conditional suppression of cellular genes: lentivirus vector-mediated drug-inducible RNA interference. J Virol 2003;77:8957–61.
40. Kita K, Kimura T, Nakamura N, Yoshikawa H, Nakano T. PI3K/Akt signaling as a key regulatory pathway for chondrocyte terminal differentiation. Genes Cells 2008;13:839–50.
41. Tsuboi H, Udagawa N, Hashimoto J, Yoshikawa H, Takahashi N, Ochi T. Nurse-like cells from patients with rheumatoid arthritis support the survival of osteoclast precursors via macrophage colony-stimulating factor production. Arthritis Rheum 2005;52:3819–28.
42. Kon S, Yokosaki Y, Maeda M, Segawa T, Horikoshi Y, Tsukagoshi H, et al. Mapping of functional epitopes of osteopontin by monoclonal antibodies raised against defined internal sequences. J Cell Biochem 2002;84:420–32.
43. Senger DR, Brown LF, Perruzzi CA, Papadopoulos-Sergiou A, Van de Water L. Osteopontin at the tumor/host interface: func-

tional regulation by thrombin-cleavage and consequences for cell adhesion. Ann N Y Acad Sci 1995;760:83–100.
44. Hata H, Sakaguchi N, Yoshitomi H, Iwakura Y, Sekikawa K, Azuma Y, et al. Distinct contribution of IL-6, TNF-α, IL-1, and IL-10 to T cell-mediated spontaneous autoimmune arthritis in mice. J Clin Invest 2004;114:582–8.
45. Nishimoto N, Kishimoto T. Interleukin 6: from bench to bedside. Nat Clin Pract Rheumatol 2006;2:619–26.
46. Svensson L, Jirholt J, Holmdahl R, Jansson L. B cell-deficient mice do not develop type II collagen-induced arthritis (CIA). Clin Exp Immunol 1998;111:521–6.
47. Dorner T, Lipsky PE. B-cell targeting: a novel approach to immune intervention today and tomorrow. Expert Opin Biol Ther 2007;7:1287–99.
48. Raychaudhuri A, Chou M, Weetall M, Jeng AY. Blockade of integrin VLA-4 prevents inflammation and matrix metalloproteinase expression in a murine model of accelerated collagen-induced arthritis. Inflammation 2003;27:107–13.

Bone 44 (2009) 71–79

Contents lists available at ScienceDirect

Bone

journal homepage: www.elsevier.com/locate/bone

High oxygen tension prolongs the survival of osteoclast precursors via macrophage colony-stimulating factor

Naomi Yamasaki, Hideki Tsuboi, Makoto Hirao, Akihide Nampei, Hideki Yoshikawa, Jun Hashimoto *

Department of Orthopedics, Osaka University Graduate School of Medicine, 2-2 Yamadaoka, Suita, Osaka 565-0871, Japan

ARTICLE INFO

Article history:
Received 20 May 2008
Revised 9 September 2008
Accepted 17 September 2008
Available online 11 October 2008

Edited by: J. Aubin

Keywords:
Destructive bone lesions
Hyperoxia
Macrophage colony-stimulating factor
Prolonged survival
Osteoclast precursor

ABSTRACT

The oxygen tension affects the function, differentiation, and transformation of various cells, including bone cells. In pathological conditions such as rheumatoid arthritis (RA), rapidly destructive arthropathy, and primary or metastatic tumors, severe bone destruction or osteolysis occurs. Abundant blood vessels are often observed around these destructive lesions. At such sites, we have confirmed the increased production of reactive oxygen species (ROS) induced by a high oxygen tension and/or oxidative stress, as well as numerous osteoclasts detectable by immunohistochemistry. These findings suggest that osteoclasts are influenced by the high oxygen tension in pathological bone lesions because the zone around blood vessels has a relatively high oxygen tension. In this study, we investigated the effects of oxygen tension on osteoclastogenesis by culturing human CD14-positive cells (osteoclast precursors) with or without osteoblast-like supporting cells (Saos-4/3 cells) under a normal oxygen tension (20% O_2) or a high oxygen tension (40% O_2). A high oxygen tension markedly prolonged the duration of osteoclast precursor formation in the presence of supporting cells, and also markedly and persistently increased the production of macrophage colony stimulating factor (M-CSF) by supporting cells. Furthermore, we found an increase of cells expressing M-CSF and cells positive for tartrate-resistant acid phosphatase (TRAP) in hypervascular destructive bone lesions of RA patients where ROS were also abundant.

© 2008 Elsevier Inc. All rights reserved.

Introduction

An increase in the number and activity of locally recruited osteoclasts is involved in various pathological states [1–3], including inflammatory arthritides such as rheumatoid arthritis (RA) and rapidly destructive arthropathy, as well as osteolytic bone tumors.

It has been demonstrated by both histological and clinical studies that these destructive bone lesions are accompanied by abundant neovascularization [4,5]. Rooney and Koizumi have shown that marked proliferation of blood vessels and the presence of neovascularization are typical histological features of RA based on the histological Rooney score [6–8]. Clinical studies using dynamic MRI have also demonstrated the enhancement of destructive bone lesions in patients with RA or bone tumors, which means that these lesions are highly vascular [9,10], and it has been suggested that the microvessel density is associated with the extent of bone destruction [3]. It has also been reported that multinucleated osteoclasts show a marked increase around regions of angiogenesis [11]. Furthermore, a recent study of the perivascular environment using a hypoxic probe demonstrated that the area around vessels is not hypoxic although hypoxia occurs further away from vessels [44]. The difference of oxygen tension between the perivascular area and the more distant region raises the question of whether a relatively high oxygen tension is associated with the recruitment of osteoclasts to sites of angiogenesis.

Recent studies have shown that the oxygen tension regulates the formation and differentiation of various bone cells, including chondrocytes, osteoblasts, osteocytes, and osteoclasts [12–15]. Such reports indicate the important influence of oxygen tension on cell biology. According to Arnett et al., hypoxia reduces the lifespan of osteoclasts, but increases their proliferation and resorption [15], while Fukuoka et al. reported that hypoxia promotes osteoclast differentiation via insulin growth factor 2 (IGF2) *in vitro* [14].

These reports raise the question of whether a high oxygen tension in hypervascular regions affect osteoclastogenesis. In this study, we investigated the influence of oxygen tension on osteoclastogenesis by culturing CD14+ cells alone or with human osteoblast-like cells.

Materials and methods

Chemicals

Recombinant human macrophage colony-stimulating factor (M-CSF) (Leukoprol) was obtained from Kyowa Hakko (Tokyo, Japan). Recombinant soluble receptor activator of nuclear factor-κB (RANKL) and osteoprotegrin (OPG) were purchased from PeproTeck (London, UK). A neutralizing antibody for human M-CSF was obtained

* Corresponding author. Fax: +81 6 6879 3559.
E-mail address: junha@ort.med.osaka-u.ac.jp (J. Hashimoto).

8756-3282/$ – see front matter © 2008 Elsevier Inc. All rights reserved.
doi:10.1016/j.bone.2008.09.015

from R & D System (Minneapolis, USA). Human parathyroid hormone 1–34 (PTH 1–34) was obtained from Peptide Institute (Osaka, Japan). Antibodies used for immunohistochemistry include a monoclonal antibody directed against human von Willebrand factor (vWF) (Dako, Glostrup, Denmark), a monoclonal antibody for human thymidine glycol (TG) (Japan Institute for the Control of Aging, Shizuoka, Japan), a polyclonal antibody targeting human M-CSF (Santa Cruz Biotechnology, Santa Cruz, CA) and a monoclonal antibody against vitronectin receptors (VNRs; human CD51/61 complex) (23C6) (Serotec, Oxford, UK).

Cell culture and osteoclast formation assay

CD14+ monocyte like cells were isolated from heparinized peripheral blood from seven healthy volunteers using anti-CD14 antibody-coated beads (Myltenyi Biotec GmbH, Germany) as described previously [16]. SaOS-4/3 cells were established from a human osteosarcoma cell line (SaOS-2) by stable transfection with human PTH/PTHrP receptor cDNA [17]. SaOS-4/3 cells support the development of human osteoclasts after stimulation by parathyroid hormone (PTH) [17,18].

For monoculture, CD14+ cells were grown in α-minimum essential medium (αMEM; Gibco BRL, Gaithersburg, MD) supplemented with 10% fetal calf serum (FCS; Hyclone, Logan, UT) in the presence of M-CSF (25 ng/ml) and RANKL (40 ng/ml). Cells were cultured under a normal oxygen tension (normoxia; 20% O_2 and 5% CO_2) or under a high oxygen tension (hyperoxia; 40% O_2 and 5% CO_2), or under a switching oxygen tension from normoxia to hyperoxia after cells began to form multinucleation, (normoxia→hyperoxia; N→H). The culture medium was exchanged every 3 days.

For coculture, CD14+ cells (3×10^4/well) were incubated with SaOs-4/3 cells (5×10^3/well) in the presence of PTH (10^{-8} M) in αMEM supplemented with 10% fetal calf serum under normoxic, hyperoxic, or N→H conditions.

After the indicated period, cells were fixed and stained for tartrate-resistant acid phosphatase (TRAP) with a TRAP staining kit (Hokudo, Hokkaido, Japan) to evaluate osteoclast formation, as described previously [16]. The number of TRAP-positive multinuclear cells with more than 3 nuclei and TRAP-positive mononuclear cells was counted every week. For immunohistochemical staining, cells were fixed with cold methanol: acetone (50: 50, volumetric ratio) for 10 min and incubated with a monoclonal antibody against VNRs, an osteoclast-associated antigen. The bound antibodies were visualized with biotinylated secondary antibodies, avidin–biotin-conjugated peroxidase, and an aminoethylcarbazole substrate kit (Histofine; Nichirei, Tokyo, Japan). Osteoclastogenesis assay were repeated using CD14+ cells of at least three donors. All experiments were triplicated.

Reverse transcription-polymerase chain reaction (RT-PCR)

Total RNA was extracted from 5×10^6 CD14+ cells with an RNeasy Kit (Qiagen, Hilden, Germany) according to the manufacturer's directions. After treatment with DNase I (Life Technologies, Rockville, MD), single-stranded cDNA was synthesized using 2 μg of each RNA sample, 100 ng of random primers, and 4 U of Omniscript Reverse Transcriptase (Qiagen) in a total reaction volume of 20 μl. Amplification was performed with 0.5 U of TaKaRa Ex Taq (Takara, Shiga, Japan). In all cases, reproducibility was confirmed by at least triplicate experiments. The primers for RANK, M-CSF, RANKL, OPG, and GAPDH have been described previously [16]. The other primer sets for DC-STAMP, Bim, Bcl2, and c-fms are shown in Table 1.

Quantitative real-time PCR

We obtained cDNA by reverse transcription as mentioned above, and proceeded to perform real-time PCR using the Roche Applied Science Light Cycler system (Roche, Basel, Switzerland). The SYBR Green assay (Roche), in which each cDNA sample was evaluated in triplicate with 20-μl reaction mixtures, was employed for all target transcripts. Expression was normalized by comparison with that of GAPDH.

Western blot analysis of M-CSF

To detect M-CSF protein, SaOs-4/3 cells were cultured for 3 or 14 days under normoxic or hyperoxic conditions. Western blot analysis was performed using whole cell lysates and 20-μl aliquots of each sample were applied. The blots were incubated with monoclonal or polyclonal antibodies for human M-CSF and then with horseradish peroxidase-coupled anti-mouse or anti-rabbit antibodies (Amersham Biosciences).

Assay of M-CSF

The M-CSF level in the conditioned medium (days 1–3, 4–6, 7–9, 10–12, and 13–16) harvested from cultures of SaOs-4/3 cells incubated under normoxic or hyperoxic conditions was measured with a human M-CSF ELISA kit (RayBiotech, Inc. Norcross, GA, USA) according to the manufacturer's instructions. Results were normalized by the number of SaOs-4/3 cells.

Inhibition of M-CSF with a neutralizing antibody

CD14+ cells (3×10^4 cells/well) were incubated with SaOs-4/3 cells (5×10^3 cells/well) in the presence of PTH (10^{-8} M) in αMEM supplemented with 10% fetal calf serum under normoxic or hyperoxia in 96-well plates for 24 h. Then neutralizing antibodies against human M-CSF were added to the cocultures after day 1 (final concentrations; 0 ng/ml=control, 50 ng/ml, 500 ng/ml), and day 14 or 25 (final concentration; 500 ng/ml). The culture medium was replaced every 3 days with the fresh medium. The number of TRAP-positive multinuclear cells with more than 3 nuclei was counted every week.

Histological examination of tissue samples

Tissue samples that included the bone-synovial interface were obtained during total knee arthroplasty from three RA patients and three osteoarthritis (OA) patients after informed consent was provided. The American College of Rheumatology criteria were used for the diagnosis of RA [19]. Tissue samples were fixed in 4%

Table 1
Sequences of polymerase chain reaction primers

	Primers (5′–3′)		Product size (bp)
	Sense	Antisense	
DC-STAMP	5′GGCCAGTGCCAAGCAGGACGAG3′	5′GCAGCTGGCACAGGGATCGTCA3′	388
Bim	5′GCAGCCGAAGACCACC3′	5′ACCGCGGTGCTGGGTC3′	151
Bcl2	5′AGCATCAGGCCGCCACAAG3′	5′CTGGAGGGCCCCAGGGTGA3′	239
c-fms	5′-TGCTGCTCCTGCTGCTATTG-3′	5′-TCAGCATCTTCACAGCCACC-3′	270

DC-STAMP = dendritic cell specific transmembrane protein.

paraformaldehyde at 4 °C for 24 h, and decalcified in 20% EDTA for 2 weeks. Next, the samples were dehydrated through an ethanol series and embedded in paraffin. Sections (4 μm thick) were cut on a microtome for TRAP and immunohistochemical analysis. The streptavidin–biotin–peroxidase complex technique with a Histofine SAB-PO kit (Nichirei) used for immunohistochemical staining. Briefly, after blocking endogenous peroxidase and nonspecific antigens, tissue sections were incubated with primary antibodies against VW, M-CSF, and TG for 24 h at 4 °C. The sections were washed with phosphate buffered saline and incubated with the secondary antibody, following by peroxidase-conjugated streptavidin (Nichirei). After a wash with phosphate buffered saline, the sections incubated with 3,3′-diaminobenzidine tetrahydrochloride (Dojindo, Kumamoto, Japan) to detect peroxidase activity.

Statistical analysis

Results are expressed as the mean±standard deviation (SD). Differences between groups were assessed by Student's *t*-test, and differences among three or more groups were assessed by post hoc analysis (Turkey–Kramer and Fisher protected least significant difference test). A p value <0.05 was considered statistically significant.

Results

TRAP-positive cells in hyperoxic and normoxic culture

To confirm osteoclast formation, we performed TRAP staining and counted the positive cells. As shown in Fig. 1A, TRAP-positive cells appeared in cultures of CD14+ cells at day 6 and the number of positive cells under hyperoxia was the same as under normoxic conditions until 14 days. In CD14+ cells monoculture with N→H, there was no effect of hyperoxia. The results obtained with vitronectin receptor (VNR) staining were the same as those for TRAP staining (data not shown). We counted the number of TRAP-positive multinuclear cells with more than 3 nuclei. There was no difference in number of these cells between two oxygen conditions (Fig. 1A-2). Next, CD14+ cells

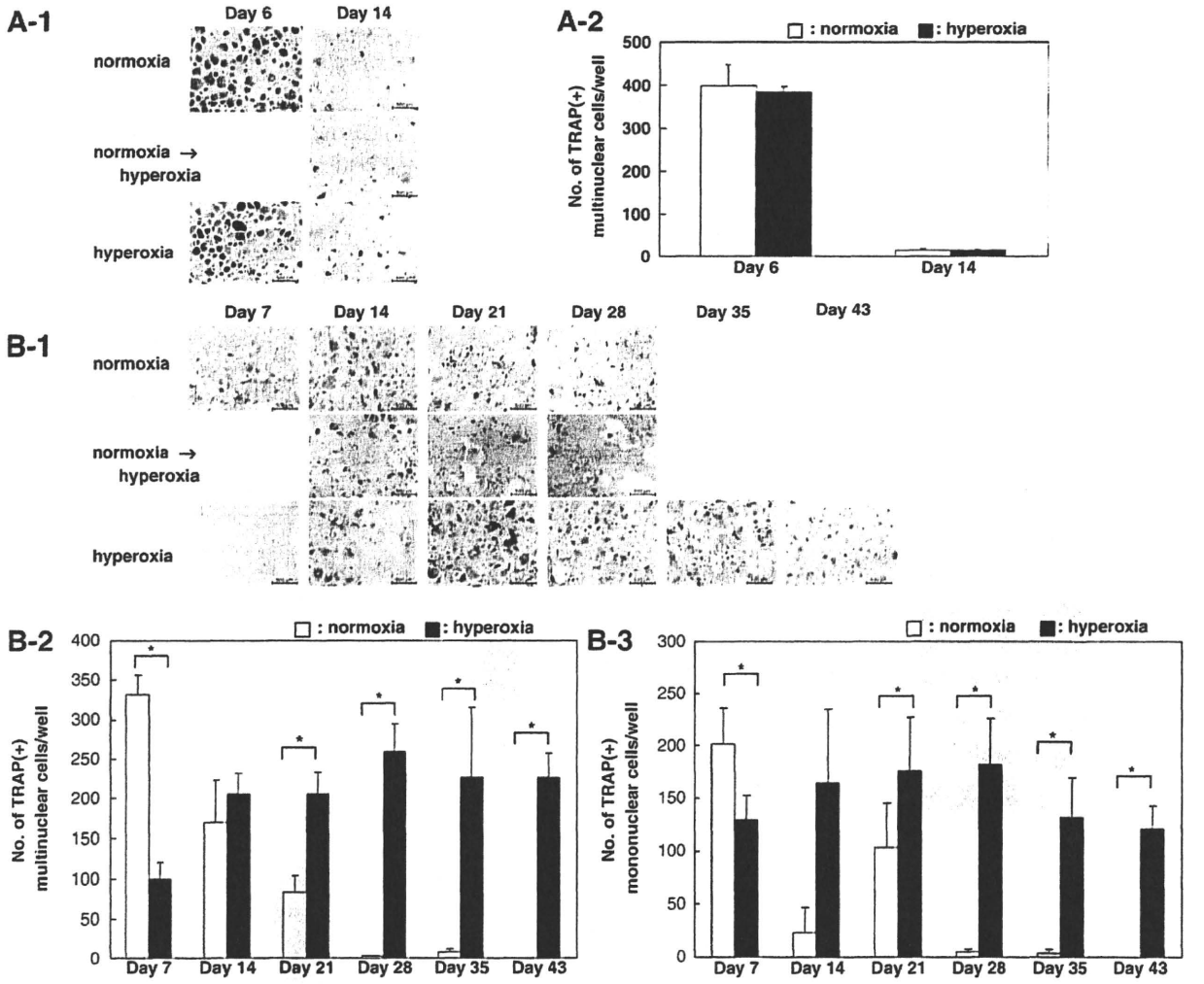

Fig. 1. Osteoclast formation from CD14+ monocytes. (A) CD14+ monocytes were cultured for 14 days with macrophage colony-stimulating factor (M-CSF: 25 ng/ml) and RANKL (40 ng/ml) under normoxic (20% O_2), normoxic to hyperoxic (N→H), or hyperoxic (40% O_2) conditions. Cultures were fixed each week and stained for tartrate-resistant acid phosphate (TRAP). Bar=500 μm (A-1). The number of TRAP-positive multinuclear cells with more than 3 nuclei was counted after 6 and 14 days of normoxia or hyperoxia (A-2). Data are shown as mean±S.D. (n=3) □, normoxia; ■, hyperoxia. (B-1) CD14+ monocytes were co-cultured with supporting cells (osteoblast-like SaOs-4/3 cells) in the presence of human parathyroid hormone (PTH: 10^{-8} M) under normoxic, normoxic to hyperoxic, or hyperoxic conditions and then fixed and stained for TRAP each week for up to 43 days. Bar=500 μm. (B-2, 3) Longer duration of osteoclast formation in cultures with supporting cells under hyperoxic conditions. (B-2) The number of TRAP-positive multinuclear cells with more than 3 nuclei in cultures with supporting cells under normoxic or hyperoxic conditions was counted each week. (B-3) The number of TRAP-positive mononuclear cells (osteoclast precursors) under normoxic or hyperoxic conditions was counted each week. *<0.001. Data are shown as mean±S.D. (n=4) □, normoxia; ■, hyperoxia.

were cultured with SaOs-4/3 cells in the presence of PTH. As shown in Fig. 1B, TRAP-positive cells formed by day 7 under normoxic conditions, but disappeared by days 14–21. With N→H culture, the newly formed CD14+ cells also disappeared by days 14–21. On other hand, TRAP-positive cells formed more slowly in hyperoxic than normoxic cultures. It took 7–14 days for CD14+ cells cocultured with SaOs-4/3 cells to be transformed into TRAP-positive cells. However, these TRAP-positive cells persisted for more than 6 weeks, a period that was three times longer than under normoxic conditions. Because an effect of hyperoxia on TRAP-positive cell formation from CD14+ cells was observed in coculture with SaOs-4/3 cells, we counted the number of TRAP-positive multinuclear cells with more than 3 nuclei and the number of TRAP-positive mononuclear cells (osteoclast precursors) in cocultures (Fig. 1B-2,3). In normoxic cultures, the number of TRAP-positive multinuclear cells began to increase on day 7, and then decreased again until the cells were rare by day 21. On the other hand, the number of TRAP-positive multinuclear cells increased after day 14 of hyperoxic culture and such cells were detected for 6 weeks (Fig. 1B-2). Transformation of TRAP-positive mononuclear cells to osteoclast precursors followed the same pattern (Fig. 1B-3).

Hyperoxia promotes M-CSF expression by SaOs-4/3 cells and c-fms expression by CD14+ cells

To investigate the mechanism underlying the above-mentioned effects of hyperoxia, we analyzed expression of the RANK (the receptor for RANKL), dendritic cell-specific transmembrane protein (DC-STAMP), c-fms (the receptor for M-CSF), Bcl2, and Bim genes on day 3 of normoxic or hyperoxic culture of CD14+ cells (Fig. 2A). RANK and DC-STAMP are important factors for osteoclastogenesis, while Bcl2 and Bim are transcription factors associated with apoptosis. There were no significant differences between normoxia and hyperoxia with regard to expression of RANK, DC-STAMP, Bcl2 and Bim (Fig. 2B-1–4), however the expression of c-fms was up-regulated under hyperoxic conditions compared with that under normoxic conditions (Fig. 2B-5). Next, we examined expression of the M-CSF, RANKL, and OPG genes by the supporting cells (osteoblast-like SaOs-4/3 cells) under normoxic or hyperoxic conditions (Fig. 3A). We found that M-CSF expression was markedly increased at day 7 and day 10 of hyperoxia (Fig. 3B-1,2). The M-CSF protein level was also increased on day 14 by Western blot analysis (Fig. 3C-1), and secretion of M-CSF into the culture medium was up-regulated after 6 days of hyperoxia according to the results of ELISA (Fig. 3C-2). RANKL expression increased in a time-dependent manner under both normoxic and hyperoxic conditions and there was no significant difference between the two levels of oxygen (Figs. 3A, B-2). OPG expression also showed no significant differences (Figs. 3A, B-3).

Inhibition of M-CSF with a neutralizing antibody abolishes hyperoxia-induced formation of TRAP-positive cells

We analyzed the influence of a neutralizing antibody directed against human M-CSF (50 ng/ml or 500 ng/ml) on cocultures of CD14+ cells and SaOs-4/3 cells under normoxic and hyperoxic conditions.

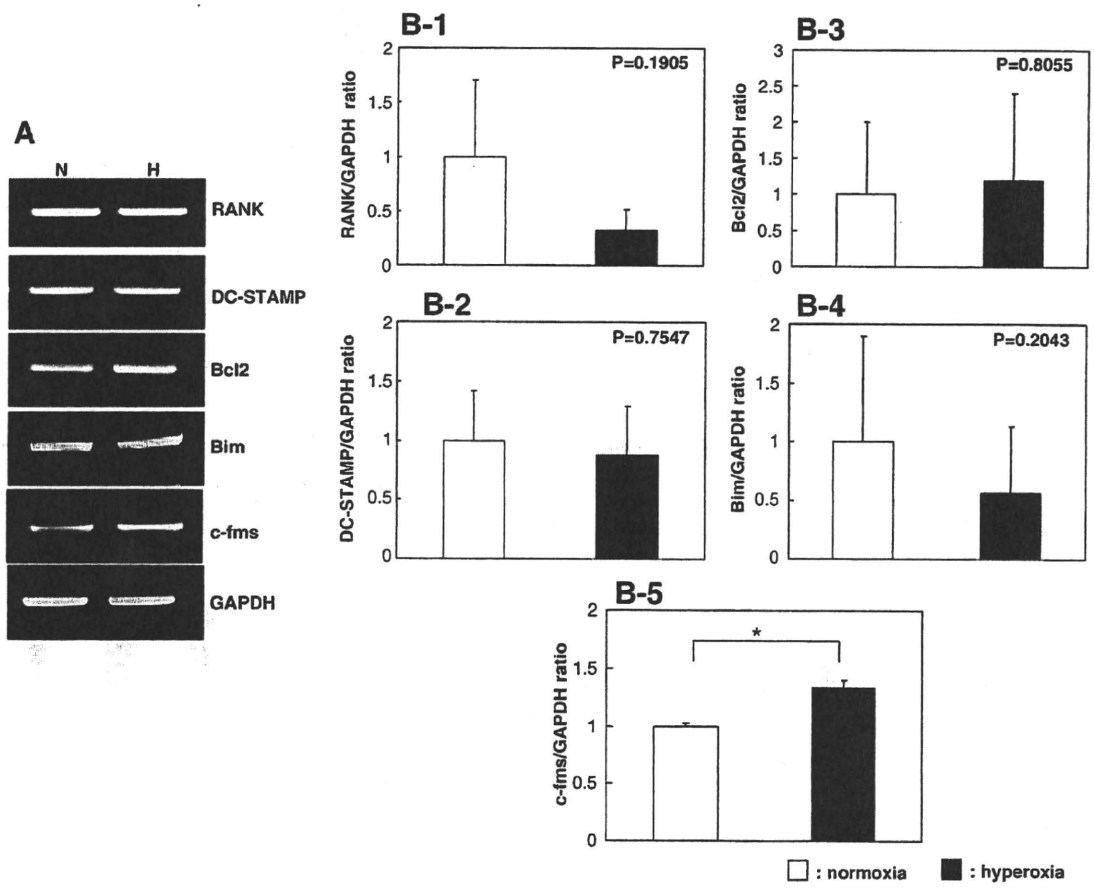

Fig. 2. Gene expression of c-fms by CD14+ monocytes increased under hyperoxia, while all other genes expression including RANK, DC-STAMP, Bcl2 and Bim did not change significantly. (A) Total RNA was extracted from CD14+ monocytes cultured under normoxic or hyperoxic conditions for 3 days, and the expression of mRNA for RANK, dendritic cell-specific transmembrane protein (DC-STAMP), Bcl2, Bim, c-fms and GAPDH was analyzed by reverse transcription polymerase chain reaction (RT-PCR). (B) Real-time PCR for RANK, DC-STAMP, Bcl2, Bim, and c-fms gene expression. Data are shown as the mean±S.D. ($n=3$) of the ratio to GAPDH for RANK (B-1), DC-STAMP (B-2), Bcl2 (B-3), Bim (B-4), and c-fms (B-5) gene expression compared with that under normoxia. Only c-fms has significantly different p value, *<0.005. □, normoxia; ■, hyperoxia.

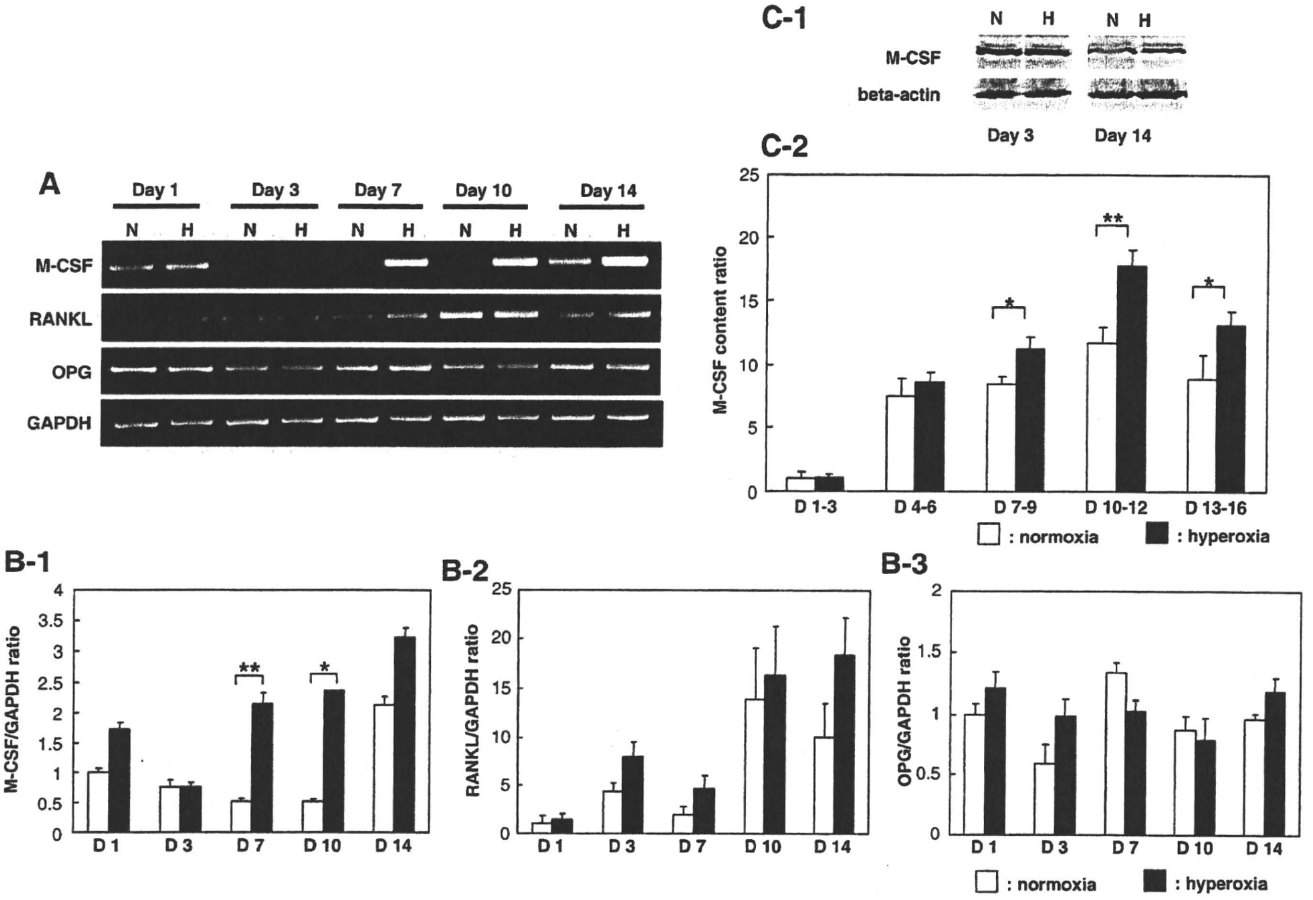

Fig. 3. Importance of M-CSF production by supporting cells for prolonged osteoclast formation under hyperoxia. SaOS-4/3 cells (5×10^6 cells/dish) were cultured for 1, 3, 7, 10, or 14 days in the presence of PTH (10^{-8} M) under normoxic or hyperoxic conditions. Total RNA was extracted from the cells, and subjected to RT-PCR to detect RANKL, OPG, and M-CSF mRNA expression. (A) Total RNA was extracted from SaOs-4/3 cells cultured under normoxic or hyperoxic conditions for 1, 3, 7, 10 or 14 days and the expression of mRNA for M-CSF, RANKL, osteoprotegrin (OPG), and GAPDH was analyzed by RT-PCR. (B) Real-time PCR for M-CSF and RANKL gene expression. Data are shown as the mean±S.D. ($n=3$) of the ratio of RANKL (B-1), M-CSF (B-2), and OPG (B-3) gene expression to GADPH compared with that under normoxic conditions on day 1. **<0.05, *<0.0005. □, normoxia; ■, hyperoxia. (C-1) SaOs-4/3 cells were cultured for 3 and 14 days under normoxic or hyperoxic conditions and lysed. The cell lysates were subjected to Western blotting with an anti-human M-CSF antibody. (C-2) Culture medium was harvested on day 3 (days 1–3), day 6 (days 4–6), day 9 (days 7–9), day 12 (days 10–12), and day 16 (days 13–16) for measurement of the M-CSF protein content by ELISA. Data are normalized by the total number of cells/well, and are shown as the mean±S.D. ($n=4$). **<0.001, *<0.01. □, normoxia; ■, hyperoxia.

After 1 week, the number of TRAP-positive multinuclear cells was decreased in a dose-dependent manner in both groups (Fig. 4A). From 2 weeks onward, the number of TRAP-positive multinuclear cells was very low under normoxic conditions, and there was no significant difference between cultures with or without M-CSF inhibition. On the other hand, the increase in the number of TRAP-positive multinuclear cells under hyperoxic conditions was partly reversed by a low dose (50 ng/ml) of anti-M-CSF antibody and was completely abolished by a high dose (500 ng/ml) at weeks 1, 2 and 3. Thus, the antibody had a dose-dependent effect.

Furthermore, this neutralizing effect in hyperoxia was decreased in case of anti-M-CSF antibody addition at weeks 2 and 3.5 when the TRAP positive cells were formed (Fig. 4B).

Increase of ROS and TRAP-positive cells at sites of bone destruction

We wanted to investigate whether hyperoxic zones exist in pathological hypervascular lesions *in vivo*, but it is too difficult to properly measure the oxygen tension of bone tissue because there are no appropriate instruments, so we measured ROS instead. We examined the distribution of vessels, ROS, and TRAP-positive multinuclear cells at sites of bone destruction in RA patients by immunohistochemistry and TRAP staining. ROS were detected with an antibody for thymidine glycol, which is one of the reactive oxygen species. It was found that vessels were abundant at the sites of bone destruction and ROS were detected in the pathological bone tissue around the vessels. In these ROS-rich areas, a large number of TRAP-positive multinuclear cells were also detected at the borders of the damaged bone (Fig. 5A).

M-CSF is associated with ROS in bone lesions

Finally, we examined the distribution of M-CSF-positive cells in the ROS-rich areas of bone destruction in RA patients. As previously described, ROS were detected at the interface of the bone lesions and M-CSF staining was also detected very strongly in the region surrounding the damaged bone (Fig. 5B-1). On the other hand, very little ROS or M-CSF was detected in OA patients (Fig. 5B-2).

Discussion

This study has provided the first evidence that a high oxygen tension promotes the survival of human osteoclast precursors via up-regulated action of M-CSF. It was previously reported that the differentiation and activity of osteoclasts were stimulated by a low oxygen tension [14,15]. We also examined the behavior of osteoclasts

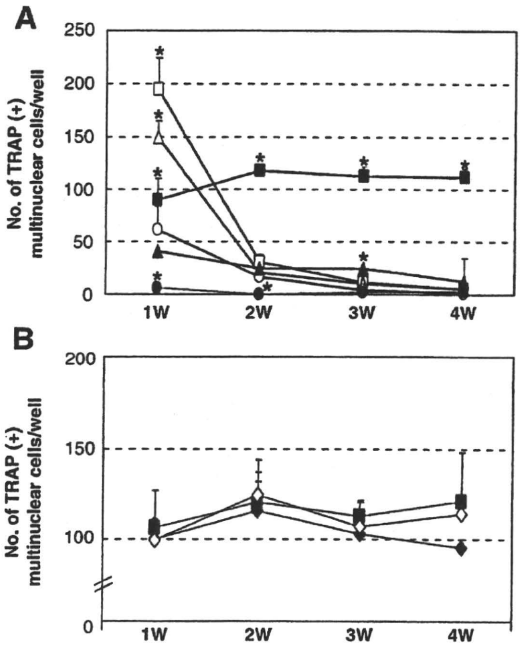

Fig. 4. M-CSF neutralizing antibody abolishes the hyperoxia-induced increase of TRAP-positive multinuclear cells with more than 3 nuclei. CD14+ monocytes were cocultured with supporting cells (SaOs-4/3 cells), and we added M-CSF neutralizing antibody against human M-CSF with increasing concentrations under normoxic or hyperoxic conditions at day 1 (final concentration; 0 ng/ml, 50 ng/ml, or 500 ng/ml) (A). The number of TRAP-positive multinuclear cells was counted each week. Data are shown as mean±S.D. (n=3). *<0.0001. □, 0 ng/ml neutralizing antibody under normoxia; ■, 0 ng/ml under hyperoxia; △, 50 ng/ml under normoxia; ▲, 50 ng/ml under hyperoxia; ○, 500 ng/ml under normoxia; ●, 500 ng/ml under hyperoxia. And we also added the antibody at day 14 or day 25 under hyperoxia (B) (final concentration; 500 ng/ml). ■, antibody was not added. ♦, the antibody was added at day 14 ◊, the antibody at day 25.

cultured under a low oxygen tension (5% O_2), and observed that the cells showed more rapid differentiation but shorter survival than cells cultured under a normal oxygen tension (data not shown), suggesting that osteoclastogenesis is influenced by the local oxygen tension. As mentioned earlier, both clinical and histological human data have suggested a possible positive interaction between hyperoxia and osteoclastogenesis, but it has not been confirmed. Accordingly, we investigated osteoclastogenesis using human CD14+ cells and previously reported monoculture or coculture systems [17,18,20–22]. Previously published data showed that osteoblasts or stromal cells are essentially involved in osteoclastogenesis through cell–cell interaction with osteoclast progenitors [52–54]. In monoculture system which is osteoclastogenesis from CD14+ cells with RANKL and M-CSF, almost all CD14+ cells are simultaneously differentiated into mature osteoclasts within 14 days and few of them remain after 2 weeks. On the other hand, CD14+ cells are maintained and/or differentiated depending on the local conditions given by osteoblast-like supporting cells in coculture system. Therefore, coculture system is considered to be closer to physiological *in vivo* conditions than monoculture. Referring to previous reports [23,45,46], we set the high oxygen tension at 40% O_2 and normal oxygen tension at 20% O_2.

Hyperoxia did not affect the number of osteoclasts and apoptosis, but up-regulated c-fms gene expression in monoculture

Interestingly, we could not detect any effect of a high oxygen tension on the number of osteoclasts in monoculture (Fig. 1A). When we assessed RANK, DC-STAMP, Bcl2, and Bim gene expression by CD14+ cells in monoculture, we could not detect any significant influence of hyperoxia on these genes, which are essential factors for the differentiation and apoptosis of osteoclasts. RANK is required for the differentiation of precursors to mature osteoclasts [24], while DC-STAMP plays an important role in macrophage fusion [25,26]. Bcl2 and Bim are associated with apoptosis, with Bcl2 being an inhibitor of apoptosis and Bim acting as a stimulator [27,28]. Meanwhile, when we assessed the expression of c-fms gene which is critical for osteoclastogenesis as the receptor of M-CSF, we detected up-regulated c-fms gene expression of CD14+ cells in hyperoxia. This result suggested that the CD14+ cells in hyperoxia could respond to M-CSF more sensitively.

Hyperoxia promoted continuous osteoclastogenesis for up to 43 days in coculture

On the other hand, the TRAP-positive cells were continuously recruited for three times longer period in hyperoxic coculture compared with normoxic coculture (Fig. 1B). The time course of osteoclast formation and the number of osteoclasts in coculture system often vary among donors as pointed out by previously published studies [48,49]. The variation of data in our study was relatively high and data in normoxia also varied in Figs. 1B-2 and 4A, however, the effect of hyperoxia on osteoclastogenesis was constant independent from donors. The differences in TRAP-positive cell number on days 21, 28, 35 and 43 between hyperoxia and normoxia were also statistically significant. These results in coculture system different from monoculture indicate that the supporting cells have an important role in osteoclastogenesis of CD14+ cells under hyperoxic conditions.

We also detected an influence of hyperoxia on M-CSF gene and protein expression by the supporting cells. M-CSF, RANKL, and OPG are produced by osteoblasts, and are essential factors for osteoclastogenesis. OPG acts as a decoy receptor for RANKL [29]. M-CSF gene expression was dramatically increased for at least 14 days under hyperoxic conditions (Fig. 3A), while RANKL and OPG were not significantly altered. Furthermore, gene expression of c-fms which is the receptor for M-CSF was increased in CD14+ cells (Fig. 2B-5). These findings suggest that M-CSF signaling from osteoblasts to CD14+ cells has an important role at a high oxygen tension rather than the RANKL-RANK system.

To determine whether hyperoxia affects osteoclast precursors or mature osteoclasts, we also cultured cells under normoxic conditions until mature osteoclasts formed (day 6), followed by a switch to hyperoxic conditions. Interestingly, exposure to hyperoxia after osteoclasts had developed showed no influence on TRAP staining (Figs. 1A-1, B-1), suggesting that a high oxygen tension does not act on mature osteoclasts but instead affects osteoclast precursors. These data agree with previously published data. M-CSF is essential for the survival of osteoclast precursors [16,30–35] and Woo et al [32] pointed out that M-CSF decreased the apoptosis of osteoclast precursors on a dose dependent manner by up-regulating Bcl-X_L which has an anti-apoptotic effect. All these observations indicated that hyperoxia continuously promoted M-CSF production by SaOs-4/3 cells and c-fms expression in CD14+ cells, which maintained viable osteoclast precursors for a longer period and resulted in the continuous recruitment of mature osteoclasts for 43 days in coculture.

Action of M-CSF is essential for continuous osteoclastogenesis in hyperoxic coculture

To confirm that hyperoxia-induced promotion of osteoclastogenesis was dependent on up-regulated action of M-CSF, we investigated the influence of an M-CSF neutralizing antibody on osteoclast precursor formation (Fig. 4A). TRAP-positive cells were almost abolished after 2 weeks of culture under normoxic conditions irrespective of the dose of antibody added on day 1 to the medium. On the other hand, osteoclast formation under hyperoxic conditions was decreased in a dose-dependent manner. These findings confirmed

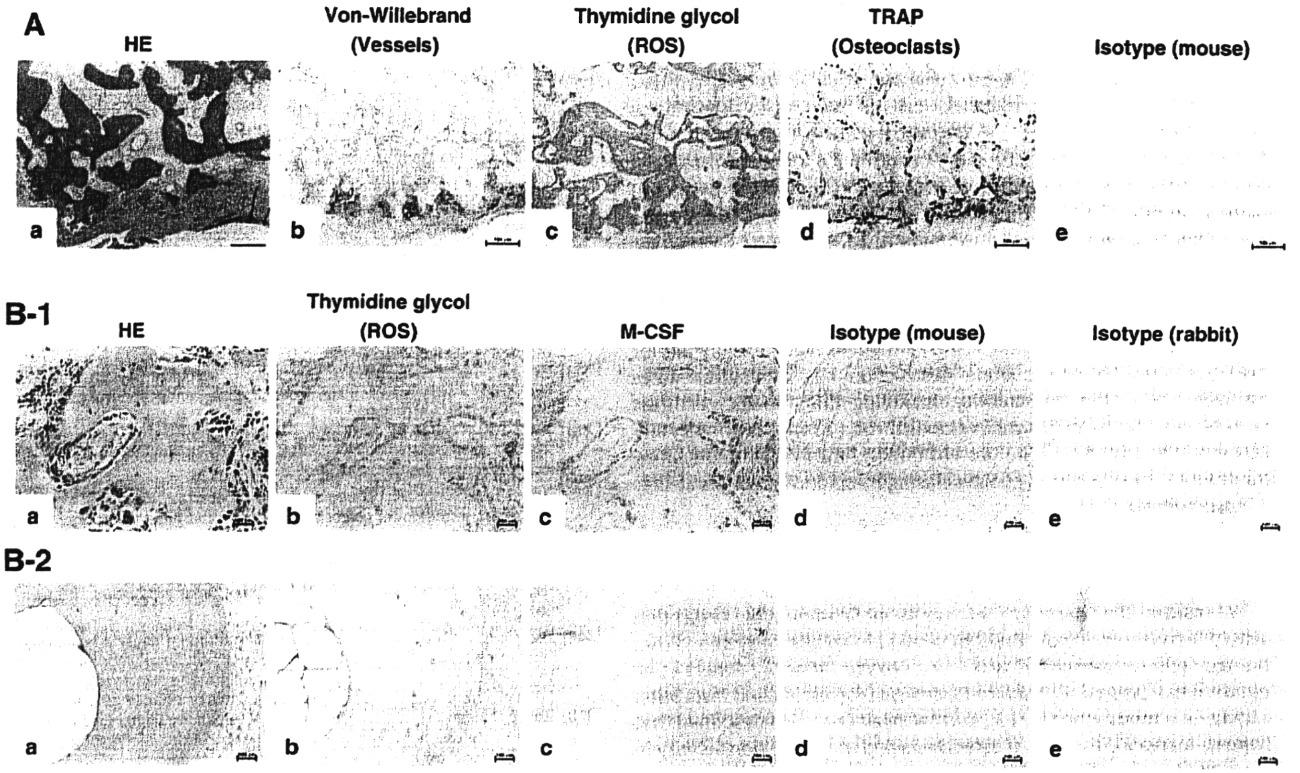

Fig. 5. (A) Localization of vessels, reactive oxygen species (ROS; thymidine glycol), and TRAP-positive cells in bone lesions. (a) H&E staining; (b) immunolocalization of von-Willebrand factor; (c) immunolocalization of ROS; (d) staining for tartrate-resistant acid phosphatase; (e) isotype control mouse IgG. Bar = 100 μm. (B) Immunolocalization of ROS and M-CSF in bone lesions of RA patients (B-1) and control tissue of OA patients (B-2). (a) H&E staining; (b) immunolocalization of ROS; (c) immunolocalization of M-CSF; (d) isotype control mouse IgG; (e) isotype control rabbit IgG. Bar = 100 μm.

that longer survival of osteoclast precursors under hyperoxic conditions was dependent on the up-regulated action of M-CSF. Interestingly, this neutralizing effect was decreased in case of the M-CSF antibody addition at 2 and 3.5 weeks after the TRAP positive cells were formed in hyperoxia (Fig. 4B). As referring to the previously published reports, M-CSF is not a critical factor for the survival of osteoclasts, while it is essential for the survival of CD14+ cells [50]. This is one of the plausible reasons why the antibody did not significantly decrease the number of TRAP positive cells after osteoclasts were already differentiated from CD14+ cells. Another possible reason is the culture-duration-dependent decrease in number of CD14+ cells because of their differentiation into osteoclasts.

However, the question arises why CD14+ cells in monoculture could not form osteoclast precursors continuously despite the addition of recombinant M-CSF and RANKL to the culture medium. TRAP-positive cells counting in monoculture showed that TRAP-positive cells appeared on day 6 and disappeared by day 14 in monoculture under both normoxia and hyperoxia (Fig. 1A-2). These data indicated that all of the CD14+ cells or osteoclast precursors had rapidly differentiated into mature osteoclasts independently of M-CSF and RANKL concentration, and few or no osteoclast precursors remain in the early days of the monoculture. This is a possible answer for the prior question. Another possible explanation is that factors other than M-CSF could be associated with the recruitment of osteoclast precursors under hyperoxia only in the coculture system. Further investigations into this issue are needed.

The association of hypervascularity, hyperoxia, and M-CSF expression

Although previous histological and clinical evaluations have shown that destructive bone lesions are accompanied by abundant neovascularization [4–10], an association among hypervascularity, a high oxygen tension, M-CSF, and osteoclasts has never been demonstrated in human tissues.

Because methods for measuring the oxygen tension in bone lesions have not been developed, we substituted the immunohistochemical detection of ROS as an indicator of the local tissue oxygen tension. Oxygen itself acts as a free radical [30], and a high oxygen tension is correlated with the production of ROS. Thus, detection of ROS implies the existence of oxidative stress [37,38], and such oxidative stress is induced in proportion to the oxygen tension [36,39,40]. We confirmed that the hyperoxic culture medium had a 2-fold higher ROS content than the normoxic medium in our vitro study (data not shown). As a result of these findings and in combination with the literature, we determined that 40% O_2 would appropriately model physiologic levels seen in RA. Therefore, we utilized ROS as a marker of a high tissue oxygen tension, and we studied the association among hypervascularity, ROS, M-CSF, and osteoclasts in bone lesions of patients with RA.

As shown in Fig. 5A, we demonstrated colocalization of hypervascularity, ROS, and TRAP-positive osteoclast-like cells on the bone surface, and furthermore, M-CSF-positive cells were increased at such abundant ROS area which is the bone destructive lesions of patients with RA (Fig. 5B-1). On the other hand, such colocalization of ROS and M-CSF was not recognized in the bone samples from OA patients (Fig. 5B-2). These histological findings indicated that hyperoxia-induced up-regulation of M-CSF production resulted in continuous osteoclast formation *in vitro*, which might reflect the actual mechanism of osteoclastic bone resorption in the hypervascular lesions of patients with RA. Enhanced production of M-CSF due to hyperoxia could provide long-term reserves of osteoclast precursors in hypervascular proliferating synovial tissue, resulting in the continuous supply of mature osteoclasts to the erosive front of affected joints in RA patients.

We previously reported that fibroblast-like synovial cells from patients with RA support the survival of osteoclast precursors via M-CSF production [16,47]. Recently, Nakano et al. also reported that M-CSF produced by RA endothelial cells is involved in osteoclastogenesis from monocytes [43]. Accordingly, enhanced production of M-CSF by hyperoxia could provide a continuing supply of osteoclast precursors that become mature osteoclasts in the affected joints of patients with RA. On the other hand, the work of Collin-Osdoby and Okada might suggest the exploration of RANKL secretion by vascular endothelial cells as a possible role [41,42]. However, our data demonstrate that RANKL expression was not altered in SaOs-4/3 cells and that RANK expression was unaltered in CD14+ cells.

Taken together, it appears that a high oxygen tension and/or oxidative stress mediates bone destruction in pathological states associated with hypervascularity, including inflammatory arthritis such as RA and rapidly destructive coxarthrosis, as well as primary and metastatic bone tumors. The present findings may provide some new insights into the processes of osteoclastogenesis and osteolysis at sites of bone pathology *in vivo*.

The limitation of this study

We realized the necessity that we should compare the resorption activity between normoxia and hyperoxia in coculture system. From the past reports associated with a low oxygen tension, Arnett et al. reported that hypoxia stimulated osteoclast formation and resorption activity in a mouse model [15], and Musylak et al. also described that hypoxia increased the size of osteoclasts and the resorption activity in a cat model [51]. These reports suggested that the oxygen tension could affect the resorption activity of osteoclasts. So, it is really interesting how hyperoxia effects on bone resorptive activity. In this study, we tried the pit formation assay in coculture system by several times, but the human coculture system is too delicate to form mature osteoclasts on dentine slices. Unfortunately we could not solve the reason and not have evaluated the resorption activity yet. So, about this problem, further studies will be needed.

In conclusion, our data suggest that a high oxygen tension dramatically prolongs osteoclast precursor formation as a result of the continuous up-regulation of M-CSF production by supporting cells and c-fms gene up-regulation in CD14+ cells. An increase of M-CSF-expressing cells and TRAP-positive cells is detected in hypervascular bone lesions along with high levels of ROS.

Acknowledgments

We would like to thank Mari Shinkawa for her excellent technical assistance, and N. Udagawa, PhD. (Matsumoto Dental University) for donating the SaOs-4/3 cells.

References

[1] Bathurst N, Sanerkin N, Watt I. Osteoclast-rich osteosarcoma. Br J Radiol 1986;59:667–73.
[2] Romas E, Gillespie MT, Martin TJ. Involvement of receptor activator of NFkappaB ligand and tumor necrosis factor-alpha in bone destruction in rheumatoid arthritis. Bone 2002;30:340–6.
[3] Yamakawa T, Sudo A, Tanaka M, Uchida A. Microvascular density of rapidly destructive arthropathy of the hip joint. J Orthop Surg (Hong Kong) 2005;13:40–5.
[4] Kindle L, Rothe L, Kriss M, Osdoby P, Collin-Osdoby P. Human microvascular endothelial cell activation by IL-1 and TNF-alpha stimulates the adhesion and transendothelial migration of circulating human CD14+ monocytes that develop with RANKL into functional osteoclasts. J Bone Miner Res 2006;21:193–206.
[5] Malemud CJ. Growth hormone, VEGF and FGF: involvement in rheumatoid arthritis. Clin Chim Acta 2007;375:10–9.
[6] Koizumi F, Matsuno H, Wakaki K, Ishii Y, Kurashige Y, Nakamura H. Synovitis in rheumatoid arthritis: scoring of characteristic histopathological features. Pathol Int 1999;49:298–304.
[7] Rooney M, Condell D, Quinlan W, Daly L, Whelan A, Feighery C, et al. Analysis of the histologic variation of synovitis in rheumatoid arthritis. Arthritis Rheum 1988;31:956–63.
[8] Matsuno H, Yudoh K, Nakazawa F, Koizumi F. Relationship between histological findings and clinical findings in rheumatoid arthritis. Pathol Int 2002;52:527–33.
[9] Hoang BH, Dyke JP, Koutcher JA, Huvos AG, Mizobuchi H, Mazza BA, et al. VEGF expression in osteosarcoma correlates with vascular permeability by dynamic MRI. Clin Orthop Relat Res 2004;426:32–8.
[10] Kajihara M, Sugawara Y, Sakayama K, Kikuchi K, Mochizuki T, Murase K. Evaluation of tumor blood flow in musculoskeletal lesions: dynamic contrast-enhanced MR imaging and its possibility when monitoring the response to preoperative chemotherapy-work in progress. Radiat Med 2007;25:94–105.
[11] Winding B, Misander H, Sveigaard C, Therkildsen B, Jakobsen M, Overgaard T, et al. Human breast cancer cells induced angiogenesis, recruitment, and activation of osteoclasts in osteolytic metastasis. J Cancer Res Clin Oncol 2000;126:631–40.
[12] Hirao M, Hashimoto J, Yamasaki N, Ando W, Tsuboi H, Myoui A, et al. Oxygen tension is an important mediator of the transformation of osteoblasts to osteocytes. J Bone Miner Metab 2007;25:266–76.
[13] Hirao M, Tamai N, Tsumaki N, Yoshikawa H, Myoui A. Oxygen tension regulates chondrocyte differentiation and function during endochondral ossification. J Biol Chem 2006;281:31079–92.
[14] Fukuoka H, Aoyama M, Miyazawa K, Asai K, Goto S. Hypoxic stress enhances osteoclast differentiation via increasing IGF2 production by non-osteoclastic cells. Biochem Biophys Res Commun 2005;328:885–94.
[15] Arnett TR, Gibbons DC, Utting JC, Orriss IR, Hoebertz A, Rosendaal M, et al. Hypoxia is a major stimulator of osteoclast formation and bone resorption. J Cell Physiol 2003;196:2–8.
[16] Tsuboi H, Udagawa N, Hashimoto J, Yoshikawa H, Takahashi N, Ochi T. Nurse-like cells from patients with rheumatoid arthritis support the survival of osteoclast precursors via macrophage colony-stimulating factor production. Arthritis Rheum 2005;52:3819–28.
[17] Matsuzaki K, Katayama K, Takahashi Y, Nakamura I, Udagawa N, Tsurukai T, et al. Human osteoclast-like cells are formed from peripheral blood mononuclear cells in a coculture with SaOS-2 cells transfected with the parathyroid hormone (PTH)/PTH-related protein receptor gene. Endocrinology 1999;140:925–32.
[18] Itoh K, Udagawa N, Matsuzaki K, Takami M, Amano H, Shinki T, et al. Importance of membrane- or matrix-associated forms of M-CSF and RANKL/ODF in osteoclastogenesis supported by SaOS-4/3 cells expressing recombinant PTH/PTHrP receptors. J Bone Miner Res 2000;15:1766–75.
[19] Arnett FC, Edworthy SM, Bloch DA, McShane DJ, Fries JF, Cooper NS, et al. The American Rheumatism Association 1987 revised criteria for the classification of rheumatoid arthritis. Arthritis Rheum 1988;31:315–24.
[20] Flanagan AM, Massey HM. Generating human osteoclasts *in vitro* from bone marrow and peripheral blood. Methods Mol Med 2003;80:113–28.
[21] Matsuzaki K, Udagawa N, Takahashi N, Yamaguchi K, Yasuda H, Shima N, et al. Osteoclast differentiation factor (ODF) induces osteoclast-like cell formation in human peripheral blood mononuclear cell cultures. Biochem Biophys Res Commun 1998;246:199–204.
[22] Kirstein B, Grabowska U, Samuelsson B, Shiroo M, Chambers TJ, Fuller K. A novel assay for analysis of the regulation of the function of human osteoclasts. J Transl Med 2006;4:45.
[23] von Zglinicki T, Saretzki G, Docke W, Lotze C. Mild hyperoxia shortens telomeres and inhibits proliferation of fibroblasts: a model for senescence? Exp Cell Res 1995;220:186–93.
[24] Teitelbaum SL. Osteoclasts: what do they do and how do they do it? Am J Pathol 2007;170:427–35.
[25] Vignery A. Macrophage fusion: the making of osteoclasts and giant cells. J Exp Med 2005;202:337–40.
[26] Kukita T, Wada N, Kukita A, Kakimoto T, Sandra F, Toh K, et al. RANKL-induced DC-STAMP is essential for osteoclastogenesis. J Exp Med 2004;200:941–6.
[27] Akiyama T, Bouillet P, Miyazaki T, Kadono Y, Chikuda H, Chung UI, et al. Regulation of osteoclast apoptosis by ubiquitination of proapoptotic BH3-only Bcl-2 family member Bim. EMBO J 2003;22:6653–64.
[28] Akiyama T, Miyazaki T, Bouillet P, Nakamura K, Strasser A, Tanaka S. In vitro and *in vivo* assays for osteoclast apoptosis. Biol Proced Online 2005;7:48–59.
[29] Nakamura M, Udagawa N, Matsuura S, Mogi M, Nakamura H, Horiuchi H, et al. Osteoprotegerin regulates bone formation through a coupling mechanism with bone resorption. Endocrinology 2003;144:5441–9.
[30] Tsurukai T, Udagawa N, Matsuzaki K, Takahashi N, Suda T. Roles of macrophage-colony stimulating factor and osteoclast differentiation factor in osteoclastogenesis. J Bone Miner Metab 2000;18:177–84.
[31] Glantschnig H, Fisher JE, Wesolowski G, Rodan GA, Reszka AA. M-CSF, TNFalpha and RANK ligand promote osteoclast survival by signaling through mTOR/S6 kinase. Cell Death Differ 2003;10:1165–77.
[32] Woo KM, Kim HM, Ko JS. Macrophage colony-stimulating factor promotes the survival of osteoclast precursors by up-regulating Bcl-X(L). Exp Mol Med 2002;34:340–6.
[33] Bouyer P, Sakai H, Itokawa T, Kawano T, Fulton CM, Boron WF, et al. Colony-stimulating factor-1 increases osteoclast intracellular pH and promotes survival via the electroneutral Na/HCO_3 cotransporter NBCn1. Endocrinology 2007;148:831–40.
[34] Okahashi N, Koide M, Jimi E, Suda T, Nishihara T. Caspases (interleukin-1beta-converting enzyme family proteases) are involved in the regulation of the survival of osteoclasts. Bone 1998;23:33–41.
[35] Tanaka S, Miyazaki T, Fukuda A, Akiyama T, Kadono Y, Wakeyama H, et al. Molecular mechanism of the life and death of the osteoclast. Ann N Y Acad Sci 2006;1068:180–6.

[36] Tuttle SW, Maity A, Oprysko PR, Kachur AV, Ayene IS, Biaglow JE, et al. Detection of reactive oxygen species via endogenous oxidative pentose phosphate cycle activity in response to oxygen concentration: implications for HIF-1alpha stability under moderate hypoxia. J Biol Chem 2007;282:36790–6.
[37] Henrotin Y, Kurz B, Aigner T. Oxygen and reactive oxygen species in cartilage degradation: friends or foes? Osteoarthr Cartil 2005;13:643–54.
[38] Correa GA, Rumpf R, Mundim TC, Franco MM, Dode MA. Oxygen tension during *in vitro* culture of bovine embryos: effect in production and expression of genes related to oxidative stress. Anim Reprod Sci 2007;104:132–42.
[39] Flandin P, Donati Y, Barazzone-Argiroffo C, Muzzin P. Hyperoxia-mediated oxidative stress increases expression of UCP3 mRNA and protein in skeletal muscle. FEBS Lett 2005;579:3411–5.
[40] Chang E, Hornick K, Fritz KI, Mishra OP, Delivoria-Papadopoulos M. Effect of hyperoxia on cortical neuronal nuclear function and programmed cell death mechanisms. Neurochem Res 2007;32:1142–9.
[41] Collin-Osdoby P, Rothe L, Anderson F, Nelson M, Maloney W, Osdoby P. Receptor activator of NF-kappa B and osteoprotegerin expression by human microvascular endothelial cells, regulation by inflammatory cytokines, and role in human osteoclastogenesis. J Biol Chem 2001;276:20659–72.
[42] Okada T, Akikusa S, Okuno H, Kodaka M. Bone marrow metastatic myeloma cells promote osteoclastogenesis through RANKL on endothelial cells. Clin Exp Metastasis 2003;20:639–46.
[43] Nakano K, Okada Y, Saito K, Tanikawa R, Sawamukai N, Sasaguri Y, et al. Rheumatoid synovial endothelial cells produce macrophage colony-stimulating factor leading to osteoclastogenesis in rheumatoid arthritis. Rheumatology (Oxford) 2007;46:597–603.
[44] Kizaka-Kondoh S, Inoue M, Harada H, Hiraoka M. Tumor hypoxia: a target for selective cancer therapy. Cancer Sci 2003;94:1021–8.
[45] Goto Y, Noda Y, Mori T, Nakano M. Increased generation of reactive oxygen species in embryos cultured in vitro. Free Radic Biol Med 1993;15:69–75.
[46] Kurosawa H, Kimura M, Noda T, Amano Y. Effect of oxygen on in vitro differentiation of mouse embryonic stem cells. J Biosci Bioeng 2006;101:26–30.
[47] Ando W, Hashimoto J, Nampei A, Tsuboi H, Tateishi K, Ono T, et al. Imatinib mesylate inhibits osteoclastogenesis and joint destruction in rats with collagen-induced arthritis (CIA). J Bone Miner Metab 2006;24:274–82.
[48] Sabokbar A, Athanasou NS. Generating human osteoclasts from peripheral blood. Methods Mol Med 2003;80:101–11.
[49] Kreja L, Liedert A, Schmidt C, Claes L, Ignatius A. Influence of receptor activator of nuclear (NF)-kappaB ligand (RANKL), macrophage-colony stimulating factor (M-CSF) and fetal calf serum on human osteoclast formation and activity. J Mol Histol 2007;38:341–5.
[50] Udagawa N, Takahashi N, Jimi E, Matsuzaki K, Tsurukai T, Itoh K, et al. Osteoblasts/stromal cells stimulate osteoclast activation through expression of osteoclast differentiation factor/RANKL but not macrophage colony-stimulating factor. Bone 1999;25:517–23.
[51] Muzylak M, Price JS, Horton A. Hypoxia induces giant osteoclasts formation and extensive bone resorption in the cat. Calcif Tissue Int 2006;79:301–9.
[52] Yasuda H, Shima N, Nakagawa N, Yamaguchi K, Kinosaki M, Goto M, et al. A novel molecular mechanism modulating osteoclast differentiation and function. Bone 1999;25:109–13.
[53] Suda T, Kobayashi K, Jimi E, Udagawa N, Takahashi N. The molecular basis of osteoclast differentiation and activation. Novartis Found Symp 2001;232:235–47.
[54] Katagiri T, Takahashi N. Regulatory mechanism of osteoblast and osteoclast differentiation. Oral Dis 2002;8:147–59.

Phytomedicine 17 (2010) 170–177

Contents lists available at ScienceDirect

Phytomedicine

journal homepage: www.elsevier.de/phymed

The fixed herbal drug composition "Saikokaryukotsuboreito" prevents bone loss with an association of serum IL-6 reductions in ovariectomized mice model ☆

T. Hattori [a,*], W. Fei [b], T. Kizawa [a], S. Nishida [b], H. Yoshikawa [a], Y. Kishida [b]

[a] Department of Orthopaedics, Osaka University Graduate School of Medicine, 2-2 Yamadaoka, Suita, Osaka 565-0871, Japan
[b] Department of Kampo Medicine, Osaka University Graduate School of Medicine, Osaka, Japan

ARTICLE INFO

Keywords:
Saikokaryukotsuboreito
Osteoporosis
IL-6
Herbal medicine

ABSTRACT

Purpose: Saikokaryukotsuboreito (SRB) is a traditional Japanese herbal medicine that has been used to treat hyperlipidemia. As some studies have shown that lipid-lowering drugs reduce osteoporosis, we investigated the effect of SRB on bone metabolism in the postmenopausal period using an ovariectomized (OVX) murine model.

Material and Methods: Fifteen aged 9 weeks female mice were divided into three groups ($n=5$ each). The OVX group and SRB group underwent bilateral ovariectomy, after which the OVX group was fed a normal diet and the SRB group fed a normal diet containing 2% SRB. The sham group underwent sham surgery and was then fed a normal diet. Eight weeks after surgery, all mice were sacrificed, and bone volume, bone histomorphometric parameters, and bone-associated phenotype were compared among the groups.

Results: Compared with the OVX group, the SRB group showed suppression of bone volume loss at the tibia (SRB group: $12.7 \pm 0.7\%$, OVX group: $9.8 \pm 0.4\%$; $p=0.005$, ANOVA) and lumbar spine (SRB group: $15.1 \pm 0.9\%$, OVX group: $11.3 \pm 0.1\%$; $p=0.031$, ANOVA). A significant decrease in eroded surface was also observed in SRB-treated ovariectomized mice compared with the OVX group ($p=0.022$, ANOVA). We also found that serum levels of interleukin (IL)-6, a primary mediator of bone resorption, in the SRB group were significantly lower than in the OVX group (SRB: 52.5 ± 6.8 pg/ml; OVX: 138.0 ± 23.1 pg/ml; $p=0.011$, ANOVA). However, unexpectedly, SRB did not affect estradiol and total cholesterol in ovariectomized mice.

Conclusion: SRB can prevent loss of bone volume and suppress serum IL-6 levels in this postmenopausal model and is a promising candidate for treatment of postmenopausal osteoporosis.

© 2010 Elsevier GmbH. All rights reserved.

Introduction

Postmenopausal osteoporosis is one of the natural consequences of aging (Riggs and Melton, 1995). It is a skeletal disorder characterized by progressive loss of bone tissue and deterioration of osseous microarchitecture which begins after natural or surgical menopause and results in an increased risk of fracture (Hodsman, 2001). Melton et al. (1989) reported that 25% of women aged 80–84 years have had at least one vertebral fracture. Fractures can reduce mobility and be very painful, thereby limiting everyday activities (Hill, 1996).

Epidemiological evidence has accumulated indicating that osteoporosis and hyperlipidemia frequently coexist, suggesting a link between bone and lipid metabolism (Ray et al., 2002). Several studies have shown that statins, which are known to have lipid-lowering effects, also have potentially beneficial effects on bone metabolism (Edwards et al., 2000; Mundy et al., 1999).

Saikokaryukotsuboreito (SRB) (Tsumura Co., Tokyo, Japan) is a traditional Japanese herbal medicine that has been used to decrease serum triglycerides and inhibit aortic intimal thickening in hypertension (Yamada et al., 1998).

This study investigated the effects of SRB on bone morphology and substances associated with bone metabolism in the postmenopausal period using an ovariectomized mouse model.

☆This study was supported in part by grants from the Ministry of Education, Science, Sports and Culture, Japan (# 19791029 [Y. K.]).

* Corresponding author. Tel.: +81 06 6879 3552; fax: +81 06 6879 3559.
E-mail address: takako-hattori@umin.ac.jp (T. Hattori).

0944-7113/$ - see front matter © 2010 Elsevier GmbH. All rights reserved.
doi:10.1016/j.phymed.2009.12.004

Materials and methods

Preparation of SRB extract, three-dimensional HPLC analysis and liquid chromatography-mass spectrometry (LC-MS/MS)

The SRB extract used was manufactured by Tsumura & Co. (Tokyo, Japan). It is composed of 10 crude drugs in fixed proportions: 5.0 g of Bupleurum Root (the root of *Bupleurum falcatum* Linne), 4.0 g of Pinelliae Tuber (the tuber of *Pinellia ternate* Breitenbach), 3.0 g of Cinnamon Bark (the bark of *Cinnamomum cassia* Blume), 3.0 g of Poria Sclerotium (the sclerotium of *Poria cocos* Wolf), 2.5 g of Scutellariae Root (the root of *Scutellaria baicalensis* Georgi), 2.5 g of Jujube (the fruit of *Zizyphus jujube* Miller var. *inermis* Rehder), 2.5 g of Ginseng (the root of *Panax ginseng* C. A. Meyer), 2.5 g of Ostreae Shell (the shell of *Ostrea gigas* Thunberg), 2.5 g of Longgu (the *Fossilia ossis mastodi*, mainly comprising calcium carbonate), and 1.0 g of Ginger (the rhizome of *Zingiber officinal* Roscoe). These crude drugs were decocted in a 10-fold volume of water for 60 min, filtered, and the filtrate spray-dried to obtain an extract yield of about 10% by weight of the original preparation. For the analysis of SRB components, the aqueous extract (0.5 g) was extracted with 20 ml of methanol under ultrasonication for 30 min. The solution was filtered through a membrane filter (0.45 μn) then subjected to high-performance liquid chromatography (HPLC) analysis. The HPLC apparatus consisted of a Shimadzu LC 10A (analysis system software: CLASS-M10A ver. 1.64, Tokyo, Japan) equipped with a multiple wavelength detector (UV 200–400 nm) (Shimadzu SPD-M10AVP, diode array detector) and an auto injector (Shimadzu CTO-10AC). HPLC conditions were as follows: column, ODS (TSK-GEL 80TS, 250 × 4.6 mm i.d., TOSOH, Tokyo, Japan); eluant, (A) 0.05 M $AcONH_4$ (pH 3.6), (B) 100% CH_3CN; linear gradient of 90% A and 10% B changing to 0% A and 100% B in 60 min (100% B was continued for 20 min); temperature, 40 °C; flow rate, 1.0 ml/min. The HPLC profile of SRB extract is shown in Fig. 1. Baicalin, baicalein, oroxylin-A and wogonin were detected as the major compounds of SRB, while cinnamic acid, saikosaponin, gingerol, and cinnamaldehyde were also observed. However, we could not detect ginsenoside, pachymic acid and beturinic acid in this HPLC analysis. Thus, we performed LC-MS/MS analysis (Fig. 2A) of Fr.1 using a system with the 1100 Agilent auto sampler, HPLC instrument (Agilent Technologies, Inc. Tokyo, Japan), and API 2000 mass spectrometer (Applied Biosystems/MDS Sciex, Tokyo, Japan). Chromatography was carried out on a reversed-phase YMC Pack ODS-AQ column (50 × 2.0 mm i.d.) with the mobile phase consisting of solvent A (10 mM ammonium formate) and solvent B (acetonitrile). A 22-min gradient was established running from 23% to 35% B over the first 4 min, 35% to 90% B over the following 5 min, and 90% B over the last 3 min before returning the system to its initial 23% B at 10 min. For qualification, Fr.1 was prepared in methanol, filtered, and transferred to the auto sampler for LC-MS/MS analysis. Standards were prepared in a mixture of methanol, 10 mM ammonium formate and acetonitrile (3:3:2). Standards and Fr.1 were injected (10 μl) into the LC-MS/MS system.

The column effluent was introduced into the mass spectrometer using electrospray ionization (ESI) in the positive and negative ion modes with nitrogen as the nebulizer and curtain gas. In the positive ion mode, the nebulizer current and temperature were 40 psi and 450 °C, respectively. The collision gas (N_2) was set at 5 psi and collision energy was 17 eV (pachymic acid), 29 eV (ginsenoside Rg1), 29 eV (ginsenoside Rf), 35 eV (ginsenoside Re), 43 eV (ginsenoside Rc), 47 eV (ginsenoside Rb1), and 43 eV (ginsenoside Rb2) with an electron multiplier voltage of

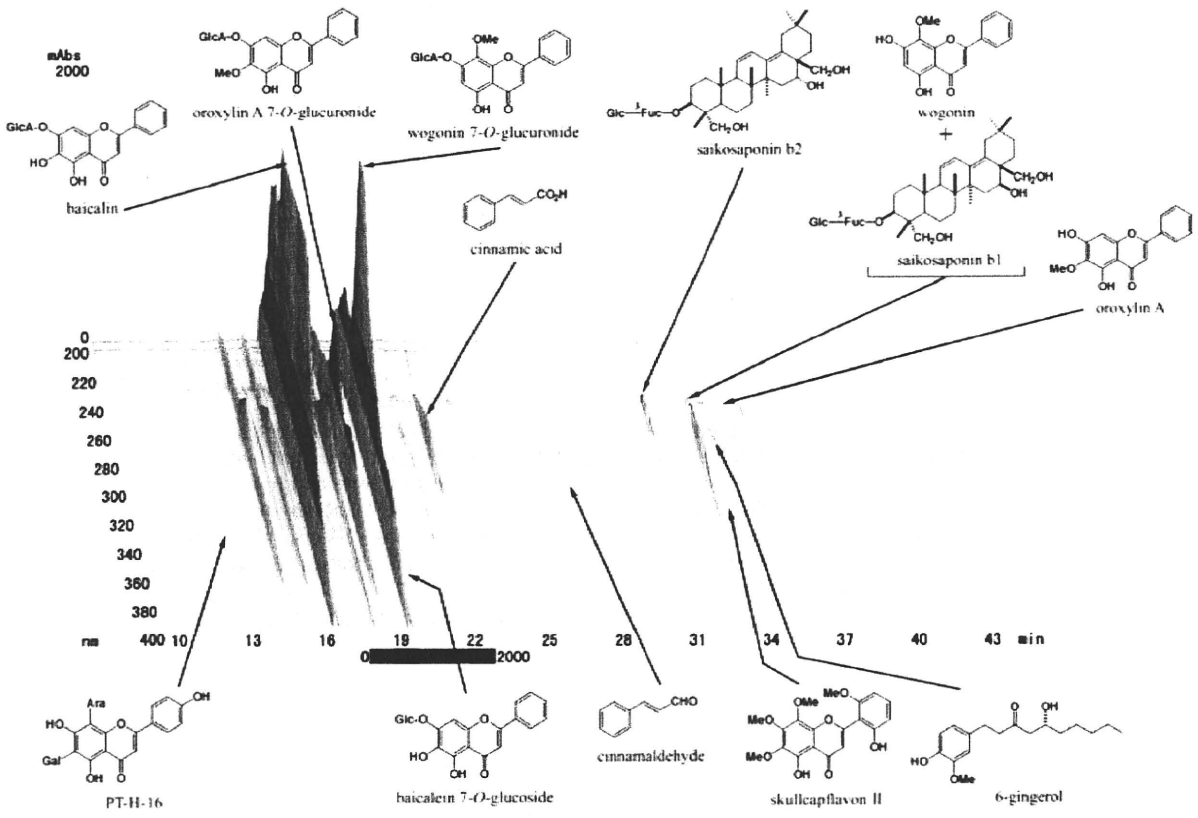

Fig. 1. Three-dimensional high performance liquid chromatography profile of SRB.

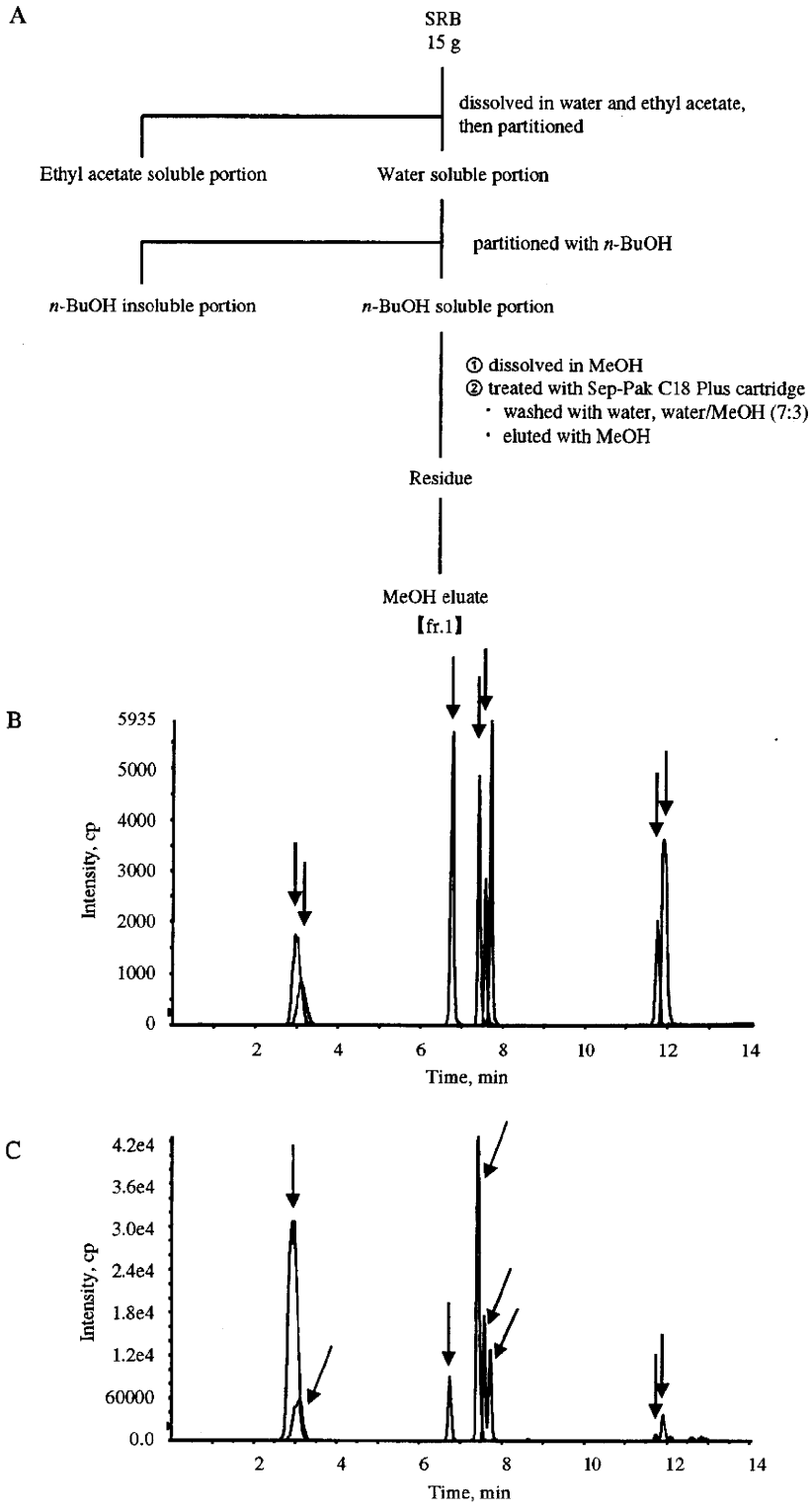

Fig. 2. Liquid chromatography-mass spectrometry profile of SRB. (A) The schema of this analysis. (B) Standard solution. Retention times (min); 2.97 (ginsenoside Rg1), 3.11 (ginsenoside Re), 6.78 (ginsenoside Rf), 7.43 (ginsenoside Rb1), 7.58 (ginsenoside Rc), 7.71 (ginsenoside Rb2), 11.77 (pachymic acid), 11.91 (betulinic acid). (C) A methanolic solution of Fr. 1. Retention times (min); 2.92 (ginsenoside Rg1), 3.10 (ginsenoside Re), 6.75 (ginsenoside Rf), 7.42 (ginsenoside Rb1), 7.57 (ginsenoside Rc), 7.72 (ginsenoside Rb2), 11.78 (pachymic acid), 11.92 (betulinic acid).

5500 V. Ginsenoside analog ions were detected as ammonium adducts [M+NH4+]+. In the negative ion mode, the nebulizer current and temperature were 20 psi and 450 °C, respectively. The collision gas (N_2) was set at 2 psi and collision energy was −24 eV (beturinic acid) with an electron multiplier voltage of −4200 V. Betulinic acid ion was detected as formate adducts

[M+HCOO−]−.The following mass transitions were used for MRM analysis: pachymic acid m/z=529/511, ginsenoside Rg1 m/z=818/423, ginsenoside Rf m/z=818/423, ginsenoside Re m/z=965/423, ginsenoside Rc m/z=1097/325, ginsenoside Rb1 m/z-1127/325, ginsenoside Rb2 m/z=1097/325 (positive ion mode), and betulinic acid m/z=501/455 (negative ion mode) (Fig. 2B and C). The LC-MS/MS system was controlled by BioAnalyst 1.4.1 software.

SRB preparation and animals

Spray-dried, water-extracted SRB powder was obtained from Tsumura & Co. C57BL/6N female mice, aged 8 weeks, were purchased from Japan Oriental Yeast Co. (Tokyo, Japan). All mice were housed under specific pathogen-free conditions with a 12 h light/dark cycle. The housing care rules and experimental protocol were approved by the Animal Care and Use Committee of Osaka University.

At the age of 9 weeks, these mice, with an average body weight 19.8 g (19.8 ± 0.3 g), were randomly divided into three groups. The first group (OVX group, n=5) and the second group (SRB group, n=5) were anesthetized with intraperitoneal injection of pentobarbital (Dainippon Sumitomo Pharma, Osaka, Japan) and bilaterally ovariectomized. For 8 weeks after surgery, the OVX group was fed a normal diet (powdered MF, Oriental Yeast Co., Ltd) and the SRB group was fed a normal diet containing 2% SRB. The last group (sham group, n=5) was sham-operated and fed a normal diet for 8 weeks after surgery. General condition, food intake, and body weight were recorded for all mice.

Micro-computed tomography (CT)

Eight weeks after surgery, at 17 weeks old, all mice were sacrificed. The tibia from each animal was sampled and the soft tissue cleaned off. The proximal metaphysis of the tibia was then scanned with a Micro-CT system (SMX-100CT-SV; Shimadzu, Kyoto, Japan) in 600 slices at a tube voltage of 45 kV and tube current of 75 μA, and the trabecular bone area (percentage of bone volume [BV] per tissue volume [TV]) was measured.

Bone histomorphometry

All mice were injected subcutaneously with 16 mg/kg calcein 7 and 2 days before being sacrificed. The lumbar spine was removed and fixed with 70% ethanol, dehydrated, and embedded in glycolmethacrylate (GMA) resin. The region studied was the secondary spongiosa, excluding the primary spongiosa 0.2 mm distal from the growth plate. Static and dynamic bone histomorphometric measurements of trabecular bone area were performed. Bone histomorphometric parameters were measured as described in the report of The American Society for Bone and Mineral Research (ASBMR) Histomorphometry Nomenclature Committee (Perfitt et al., 1987).

Serum analysis

Immediately after sacrifice, blood was withdrawn from the abdominal aorta. Serum estradiol and interleukin (IL)-6 levels were measured using an enzyme-linked immunoassay kit (estradiol: Cayman Chemical, Ann Arbor, MI, USA; IL-6: Bender Medsystems, Vienna, Austria). Total cholesterol was measured using a Wako L-type CHO H kit (Wako Pure Chemical Industries, Osaka, Japan). Sensitivities of these assays were as follows: estradiol, 20 pg/ml; total cholesterol, 0.4 mg/dl; IL-6, 12 pg/ml.

Statistical analysis

All data are expressed as the mean ± standard error of the mean (SEM). Statistical analysis was performed using JMP IN 5.1 (SAS Institute, Cary, NC, USA). Statistical significance of comparisons was determined by one-way analysis of variance (ANOVA). Values of $p < 0.05$ were considered to indicate statistical significance.

Results

SRB had no adverse effects

All mice survived after ovariectomy or sham operation. No mice in the SRB group experienced side effects, including weight loss or unusual activity. There was no significant difference in food intake per day among the three groups (OVX: 4.1 ± 1.1 g; SRB: 4.0 ± 0.8 g; sham: 3.5 ± 0.3 g; one-way ANOVA, p=0.16). There was also no significant difference in body weight among the three groups (OVX: 29.8 ± 0.4 g; SRB: 29.5 ± 0.8 g; sham: 28.1 ± 0.5 g; one-way ANOVA, p=0.14) at the end of the experiment.

SRB suppressed loss of tibial trabecular bone volume in ovariectomized mice

To investigate the role of SRB in bone metabolism, we determined structural changes in trabecular bone with micro-CT. Fig. 3A–C show representative micro-CT images of the proximal tibia of the three groups, indicating deterioration of the microarchitecture in the OVX group compared with the SRB group. Fig. 3D shows that trabecular bone volume in the SRB group was significantly greater than in the OVX group (OVX group: 9.8 ± 0.4%; SRB group: 12.7 ± 0.7%; sham group: 17.2 ± 1.2% one-way ANOVA, p=0.0001). Although the differences between the SRB and sham group were statistically significant, bone volume in the SRB group tend to be maintained closer to levels in the sham group compared with the OVX group.

SRB suppressed loss of trabecular bone volume of lumbar vertebrae in ovariectomized mice

Bone histomorphometric parameters at the end of the experiment are shown in Fig. 4. Bone volume of the lumbar vertebrae was significantly larger in the SRB group than in the OVX group (one-way ANOVA, p=0.0015, Fig. 4A). Bone volume in the SRB group did not differ significantly from that in the sham group. Trabecular bone number (Tb.N) and trabecular bone space (Tb.Sp) in the SRB group were closer to sham group readings than those in the OVX group, although the differences between the SRB and sham group were statistically significant (Tb.N, one-way ANOVA, p=0.0014; Tb.Sp, p=0.0008; Fig. 4C and D).

The ratios of osteoblast surface (Ob.S)/bone surface (BS) and osteoclast surface (Oc.S)/BS in the SRB group tended to be smaller than those in the OVX group, but there were no significant differences between these two groups (Ob.S/BS: one-way ANOVA, p=0.81; Oc.S/BS: p=0.29; Fig. 4E and H).

The eroded surface (ES)/BS (%) was significantly smaller in the SRB group than in the OVX group (one-way ANOVA, p=0.054, Fig. 4F). No significant difference was observed between the SRB and OVX groups for mineral apposition rate (MAR) or bone formation rate (BFR) (Fig. 4I and K).

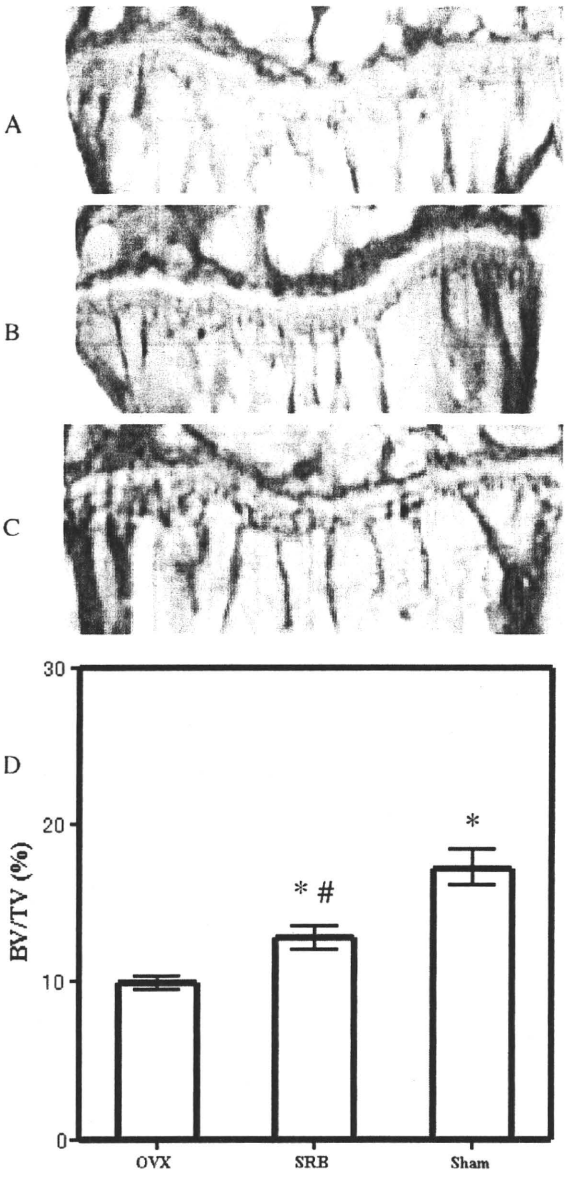

Fig. 3. (A–C) Three-dimensional micro-CT images of proximal tibias from C57BL/6N mice. (A) OVX group, (B) SRB group, and (C) sham group. (D) Bone volume (%) of the proximal metaphyseal region of the tibia, as measured by micro-CT. Data are expressed as mean ± SEM. *; significant difference compared with OVX group, #; significant difference compared with sham group.

SRB downregulated serum IL-6 level in ovariectomized mice

Next, we examined the effect of SRB on serum levels of estradiol, total cholesterol, and IL-6, because these are relevant to bone metabolism and change drastically in the perimenopausal period. Serum estradiol level was significantly higher in the sham group than in either the OVX or SRB groups (OVX: 9.5 ± 0.6 pg/ml; SRB: 8.7 ± 0.6 pg/ml; sham: 33.7 ± 3.9 pg/ml; one-way ANOVA, $p < 0.0001$). However, there was no significant difference in serum estradiol levels between the SRB and OVX groups. Total cholesterol was significantly lower in the sham group than in either the OVX or SRB groups, and, unexpectedly, cholesterol level was not suppressed in the SRB group (OVX: 87.5 ± 5.2 mg/ml; SRB: 85.3 ± 4.3 mg/ml; sham: 70.6 ± 7.4 mg/ml; one-way ANOVA, $p = 0.01$). Serum IL-6 levels were significantly lower in the SRB and sham groups than in the OVX group; IL-6 level did not increase in the SRB group despite ovariectomy (OVX: 138.0 ± 23.1 pg/ml; SRB: 52.5 ± 6.8 pg/ml; sham: 99.7 ± 19.3 pg/ml; one-way ANOVA, $p = 0.02$).

Discussion

Estrogen deficiency in postmenopausal women results in enhanced bone resorption that leads to osteoporosis. For treatment and prevention of osteoporosis, raloxifene and the bisphosphonates are currently the preferred therapy. These agents effectively decrease bone resorption and increase bone mineral density, and reduce the risk of vertebral and other fractures (Delmas et al., 1997; Poole and Compston, 2007); however, they are associated with an increase in the incidence of fatal stroke, venous thromboembolic events (Barrett-Connor et al., 2006), osteonecrosis of the jaw, and gastrointestinal side effects (Ruggiero et al., 2004; Turbi et al., 2004). Hence, further therapeutic options for osteoporosis are needed.

In recent years, various Kampo medicines have been studied for their preventive effects on osteoporosis. Hachimijiogan, Juzentaihoto and Unkeito can improve ovarian function, so these three formulae were indicated to be useful for preventing postmenopausal osteoporosis (Hidaka et al., 1997; Okamoto et al., 1998; Chen et al., 2005). Yao et al. also reported that Goshajinkigan reduced trabecular bone loss as assessed by micro-CT in ovariectomized rats (Yao et al., 2007). Hidaka's group measured bone mineral density (BMD) and performed scanning electron micrography (SEM) in rats with osteoporosis and reported that Chujoto had similar efficacy to 17β-oestradiol in treatment (Hidaka et al., 1999). Dae-bo-won-chun is also reportedly effective in preventing bone loss, and it suppresses the mechanical weakening of the femoral neck in ovariectomized rats (Chae et al., 2001). In addition, several *in vitro* studies have clarified how Kampo medicines work on bone metabolism (Li et al., 1998; Li et al., 1999; Shi et al., 2006). These studies indicate that several Kampo medicines can prevent osteoporosis.

Some studies have shown that lipid-lowering drugs reduce osteoporosis (Edwards et al., 2000; Mundy et al., 1999; Wang et al., 2000). Since SRB was reported to have an effect on hyperlipidemia (Yamada et al., 1998), we herein tested the hypothesis that SRB reduces bone loss in a postmenopausal model.

Using micro-CT, we showed that bone volume of the proximal tibia of SRB-treated mice was significantly greater than that of mice in the OVX group. Bone histomorphometric analysis of lumbar vertebrae also showed that SRB prevented the ovariectomy-induced loss of bone volume. In the SRB group, restoration of bone mass was more prominent for the spine than for the tibia. This finding was supported by previous studies, which revealed that bone loss in OVX rats was more rapid at appendicular bone sites (e.g., the tibia) than at axial bone sites (e.g., the lumbar vertebra) (Cui et al., 2004; Ke et al., 1995). A significant decrease in eroded surface and trends toward decreased osteoblast and osteoclast surfaces were also observed in SRB-treated ovariectomized mice compared with mice that underwent ovariectomy alone. These findings imply that SRB suppressed the rapid increase in bone turnover after ovariectomy. Bone formation indices such as MAR and BFR were not altered by SRB in ovariectomized mice. Taken together, these findings suggest that the protective effects of SRB on bone in ovariectomized mice are likely due to a suppression of bone resorption.

Unkeito, another Kampo medicine, has an estrogen-like effect and prevents the development of bone loss induced by ovariectomy in rats (Chen et al., 2005). However, the present study showed that SRB did not alter serum estradiol in ovariectomized mice. Although

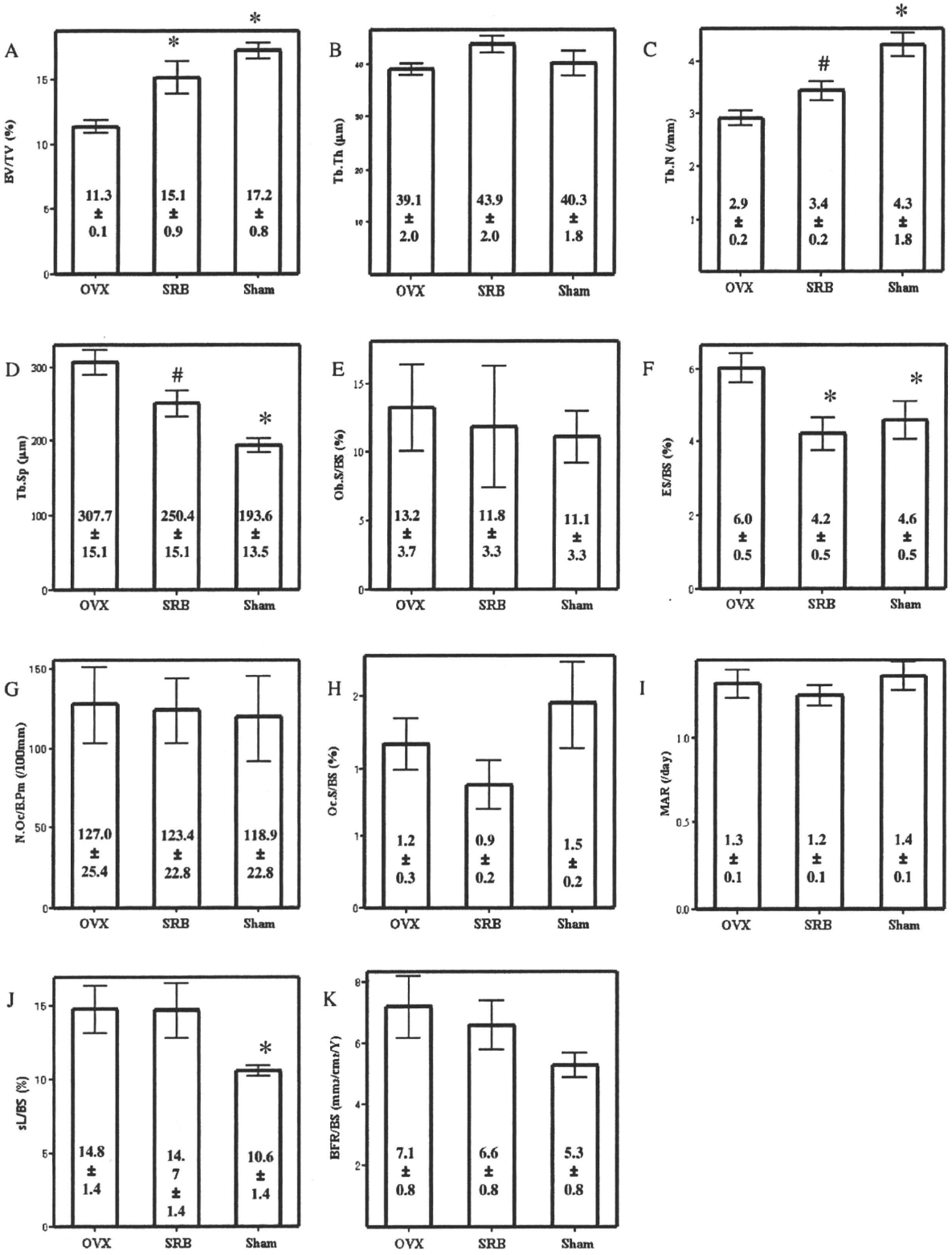

Fig. 4. Histomorphometric analysis of trabecular bone in the lumbar spine. (A) bone volume/tissue volume (BV/TV); (B) trabecular thickness (Tb.Th); (C) trabecular number (Tb.N); (D) trabecular space (Tb.Sp); (E) osteoblast surface/bone surface (Ob.S/BS); (F) eroded surface/bone surface (ES/BS); (G) osteoblast number/bone perimeter (N.Oc/BPm); (H) osteoclast surface/bone surface (Oc.S/BS); (I) mineral apposition rate (MAR); (J) mineralizing surface; single labeled surface/bone surface (sL/BS); (K) bone formation rate/bone surface (BFR/BS). Data are expressed as mean ± SEM. *; significant difference when compared with OVX group, #; significant difference when compared with sham group.